

1 **The influence of light on nitrogen cycling and the primary nitrite maximum in a seasonally**  
2 **stratified sea**

3  
4 Katherine RM Mackey<sup>1,2,3</sup>, Laura Bristow<sup>4</sup>, David R Parks<sup>5</sup>, Mark A Altabet<sup>4</sup>, Anton F Post<sup>6</sup>,  
5 and Adina Paytan<sup>3</sup>

6  
7 <sup>1</sup> Corresponding author, [kmackey@stanford.edu](mailto:kmackey@stanford.edu), 301.356.4041

8 <sup>2</sup> Department of Civil and Environmental Engineering, Stanford University, Stanford, CA 94305

9 <sup>3</sup> Institute of Marine Sciences, University of California Santa Cruz, Santa Cruz, CA 95064

10 <sup>4</sup> School for Marine Science and Technology, University of Massachusetts Dartmouth, New  
11 Bedford, MA 02744

12 <sup>5</sup> Stanford Shared FACS Facility, Stanford University School of Medicine, Stanford, CA 94305

13 <sup>6</sup> The Josephine Bay Paul Center for Comparative Molecular Biology and Evolution, Marine  
14 Biological Laboratory, Woods Hole, MA 02543

15

16

17 **Key words:**

18 Nitrogen cycle, primary nitrite maximum, nitrification, light, mixing and stratification, spring  
19 bloom

20

21 **Regional index terms:**

22 Middle East, Red Sea, Gulf of Aqaba, open ocean

23     **Acknowledgements**

24             We thank our colleagues at the Interuniversity Institute for Marine Science in Eilat, Israel  
25 for assisting in data collection and providing laboratory space and equipment during the study. C.  
26 Danford and R. Foster assisted with sampling, D. Iluz provided PAR data, S. Monismith  
27 provided mixing rates, and T. Rivlin and M. Chernichovsky assisted with sampling and nutrient  
28 analyses. Monthly monitoring data was accessed from <http://www.iui-eilat.ac.il/NMP>. This  
29 research was supported under the North Atlantic Treaty Organization (NATO) Science for Peace  
30 Grant SfP 982161 to AP and AFP, a grant from the Koret Foundation to AP, a National Science  
31 Foundation Biological Oceanography grant to AP, the Israel Science Foundation grant 135/05 to  
32 AFP, and research grant 8330-06 from the Geological Society of America to KRMM. KRMM  
33 was supported through the National Science Foundation (NSF) Graduate Research Fellowship  
34 Program and the Department of Energy (DOE) Global Change Education Program.  
35

36 **Abstract**

37 In the seasonally stratified Gulf of Aqaba Red Sea, both  $\text{NO}_2^-$  release by phytoplankton  
38 and  $\text{NH}_4^+$  oxidation by nitrifying microbes contributed to the formation of a primary nitrite  
39 maximum (PNM) over different seasons and depths in the water column. In the winter and  
40 during the days immediately following spring stratification,  $\text{NO}_2^-$  formation was strongly  
41 correlated ( $R^2=0.99$ ) with decreasing irradiance and chlorophyll, suggesting that incomplete  
42  $\text{NO}_3^-$  reduction by light limited phytoplankton was a major source of  $\text{NO}_2^-$ . However, as  
43 stratification progressed,  $\text{NO}_2^-$  continued to be generated below the euphotic depth by microbial  
44  $\text{NH}_4^+$  oxidation, likely due to differential photoinhibition of  $\text{NH}_4^+$  and  $\text{NO}_2^-$  oxidizing  
45 populations. Natural abundance stable nitrogen isotope analyses revealed a decoupling of the  
46  $\delta^{15}\text{N}$  and  $\delta^{18}\text{O}$  in the combined  $\text{NO}_3^-$  and  $\text{NO}_2^-$  pool, suggesting that assimilation and nitrification  
47 were co-occurring in surface waters. As stratification progressed, the  $\delta^{15}\text{N}$  of particulate N below  
48 the euphotic depth increased from -5‰ to up to +20‰.

49 N uptake rates were also influenced by light; based on  $^{15}\text{N}$  tracer experiments,  
50 assimilation of  $\text{NO}_3^-$ ,  $\text{NO}_2^-$ , and urea was more rapid in the light ( $434\pm 24$ ,  $94\pm 17$ , and  $1194\pm 48$   
51  $\text{nmol N L}^{-1} \text{ day}^{-1}$  respectively) than in the dark ( $58\pm 14$ ,  $29\pm 14$ , and  $476\pm 31$   $\text{nmol N L}^{-1} \text{ day}^{-1}$   
52 respectively). Dark  $\text{NH}_4^+$  assimilation was  $314\pm 31$   $\text{nmol N L}^{-1} \text{ day}^{-1}$ , while light  $\text{NH}_4^+$   
53 assimilation was much faster, resulting in complete consumption of the  $^{15}\text{N}$  spike in less than 7  
54 hour from spike addition. The overall rate of coupled urea mineralization and  $\text{NH}_4^+$  oxidation  
55 ( $14.1\pm 7.6$   $\text{nmol N L}^{-1} \text{ day}^{-1}$ ) was similar to that of  $\text{NH}_4^+$  oxidation alone ( $16.4\pm 8.1$   $\text{nmol N L}^{-1}$   
56  $\text{day}^{-1}$ ), suggesting that for labile dissolved organic N compounds like urea, mineralization was  
57 not a rate limiting step for nitrification. Our results suggest that assimilation and nitrification  
58 compete for  $\text{NH}_4^+$  and that N transformation rates throughout the water column are influenced by  
59 light over diel and seasonal cycles, allowing phytoplankton and nitrifying microbes to contribute  
60 jointly to PNM formation. We identify important factors that influence the N cycle throughout  
61 the year, including light intensity, substrate availability, and microbial community structure.  
62 These processes could be relevant to other regions worldwide where seasonal variability in  
63 mixing depth and stratification influence the contributions of phytoplankton and non-  
64 photosynthetic microbes to the N cycle.

65

## 66 1. Introduction

67 Nitrogen (N) is a limiting nutrient for primary producers in many marine environments,  
68 and nitrogen compounds are important energy sources for marine microbes. Nitrogen cycling in  
69 the surface ocean involves several key N transformation pathways (**Fig. 1**). The major source of  
70 new (external) N is the supply of nitrate ( $\text{NO}_3^-$ ) from deep mixing, advection, or diffusion (Zehr  
71 and Ward 2002).  $\text{N}_2$  fixation and atmospheric deposition also provide new bioavailable N for  
72 phytoplankton growth in some regions (Sañudo-Wilhelmy et al. 2001; Gruber and Sarmiento  
73 1997; Montoya et al. 2004; Duce et al. 2008). Phytoplankton assimilate  $\text{NH}_4^+$ ,  $\text{NO}_3^-$ , and  $\text{NO}_2^-$ ,  
74 collectively referred to as dissolved inorganic N (DIN), into their biomass during autotrophic  
75 growth, forming particulate and dissolved organic N (PON and DON) compounds. Organic N is  
76 released directly into the environment during cell lysis or excretion, and can be remineralized  
77 back to  $\text{NH}_4^+$  by microbes during ammonification (Dugdale and Goering 1986; Hollibaugh and  
78 Azam 1983; Stepanauskas et al. 1999). To complete the cycle,  $\text{NH}_4^+$  is converted first to  $\text{NO}_2^-$   
79 and then  $\text{NO}_3^-$  in successive oxidation reactions by different groups of marine nitrifiers during  
80 nitrification (Wuchtner et al. 2006; Ward and Carlucci 1985). In turn,  $\text{NO}_3^-$  can be converted to  
81  $\text{NO}_2^-$  through incomplete  $\text{NO}_3^-$  reduction by phytoplankton (Collos 1998), or through photo-  
82 reduction (Zafiriou and True 1979). Other N transformation processes like denitrification  
83 (Gruber and Sarmiento 1997) and anaerobic  $\text{NH}_4^+$  oxidation (Francis et al. 2007) also contribute  
84 to N cycling in anoxic marine environments, but generally do not occur in oxygenated waters.

85 Recent findings have demonstrated that the marine N cycle is more complex than  
86 previously understood. For example, certain non-photosynthetic microbes possess genes for  $\text{NO}_3^-$   
87 ,  $\text{NO}_2^-$ , and  $\text{NH}_4^+$  uptake similar to phytoplankton, and are a potentially important “sink” for DIN  
88 that is independent of light (Allen et al. 2001; Allen et al. 2005; Cai and Jiao 2008; Starkenburg  
89 et al. 2006; Tupas et al. 1994). Likewise, certain phytoplankton utilize DON to satisfy their N  
90 demands, similar to heterotrophs (Palenik and Morel 1990; Moore et al. 2002; Zubkov et al.  
91 2003). These findings suggest that more overlap exists in the types of N substrates taken up by  
92 phytoplankton and non-photosynthetic microbes than previously believed.

93 The conditions and setting where the various processes of the N cycle occur has also been  
94 expanded. For example, some marine nitrifier populations are inhibited by light, and thus  
95 nitrification was thought to be confined to deeper waters (Olsen 1981). However, high  
96 nitrification rates within surface waters were observed using  $^{15}\text{N}$  tracers (Ward et al. 1989) or  
97 calculated using natural abundance  $^{15}\text{N}$  and  $^{18}\text{O}$  data for  $\text{NO}_3^-$  (Wankel et al. 2007). Nitrification  
98 may therefore occur throughout the water column in some locations.

99 Despite the complexity of the N cycle, several important characteristics remain apparent.  
100 The N cycle comprises numerous N reservoirs ( $\text{NO}_3^-$ ,  $\text{NO}_2^-$ , DON, etc), and their concentrations  
101 and vertical distributions in the water column are affected by physical, chemical and biological  
102 factors. Each reservoir may have numerous sources and sinks, some of which have yet to be  
103 characterized. Importantly, the dynamic nature of the N cycle, with multiple reactions taking  
104 place simultaneously, may result in large fluxes into and out of each reservoir. Yet these fluxes  
105 are difficult to quantify by measuring concentration changes alone because the turnover can be  
106 very rapid and shuttle N back and forth between reservoirs. Therefore, the standing stock of any  
107 N compound in the water column can be constant or very low even though turnover (production  
108 and consumption) may be rapid.

109 Changes in the concentrations of certain N compounds can occur if fluxes into and out of  
110 a reservoir become unbalanced. An example of this type of phenomenon is the accumulation of  
111  $\text{NO}_2^-$  in a stratified water column when  $\text{NO}_2^-$  production exceeds its consumption, leading to

112 formation of a primary  $\text{NO}_2^-$  maximum (PNM, Lomas & Lipschultz 2006). Two mechanisms  
113 have been proposed to describe how  $\text{NO}_2^-$  maxima form. The first entails uncoupled oxidation of  
114  $\text{NH}_4^+$  and  $\text{NO}_2^-$  during nitrification which leads to  $\text{NO}_2^-$  buildup if the microbial populations  
115 responsible for each step are spatially segregated within the water column. This could occur if  
116 the populations have different sensitivities to light (Olsen 1981; Guerro and Jones 1996) or  
117 different demands for substrate. The second process involves  $\text{NO}_2^-$  production during incomplete  
118  $\text{NO}_3^-$  assimilation by phytoplankton, particularly when light stressed (Collos 1998; Lomas and  
119 Gilbert 1999; Lomas and Lipschultz 2006).  $\text{NO}_2^-$  release by phytoplankton could occur if the cell  
120 does not receive enough light energy to complete the reduction of  $\text{NO}_2^-$  into  $\text{NH}_4^+$  (Collos 1998),  
121 or in response to rapidly changing light conditions, possibly as a photoprotective mechanism  
122 (Lomas and Gilbert 2000). Nitrite maxima throughout the world's oceans are generally attributed  
123 to one of these two processes (Lipschultz & Lomas 2006 and references therein), although Dore  
124 and Karl (1996a,b) showed that vertical separation of reductive and oxidative microbial  
125 processes contributes to PNM formation in the Pacific Ocean. Whether these processes co-occur  
126 in other locations and, if so, how physical factors influence which process dominates and at what  
127 depth in the water column is not clear.

128 Isotopic analysis of coupled nitrogen ( $\delta^{15}\text{N}$ ) and oxygen ( $\delta^{18}\text{O}$ ) in  $\text{NO}_3^-$  can be used for  
129 discriminating between biologically mediated N transformation processes, such as those giving  
130 rise to the PNM, since each process imparts a unique isotopic signature to both the N and O  
131 composition of the sample (Casciotti et al. 2002; Wankel 2006). This is a result of isotope  
132 fractionation, which occurs because organisms preferentially take up the light isotopes of O and  
133 N, leaving the heavier O and N isotopes in the residual substrate, i.e.  $\text{NO}_3^-$ . In processes such as  
134 assimilation (and denitrification under anaerobic conditions), the  $\delta^{18}\text{O}_{\text{NO}_3}$  and  $\delta^{15}\text{N}_{\text{NO}_3}$  are  
135 viewed to be coupled, as they increase proportionally as  $\text{NO}_3^-$  is consumed, with an O:N ratio of  
136 isotope effects of  $\sim 1$  (Granger et al, 2004 and 2008).

137 In contrast, nitrification results in the decoupling of  $\delta^{18}\text{O}$  and  $\delta^{15}\text{N}$  of nitrate and as a  
138 result values will plot along a line with a slope greater than 1. This decoupling is a result of the  
139 processes of assimilation and nitrification competing for the  $\text{NH}_4^+$  substrate (Wankel 2007). The  
140 difference between the isotope effect of nitrification and that of assimilation will determine the  
141 isotopic composition of the  $\text{NO}_3^-$  returned to the N pool. The greater the difference between the  
142 isotope effects of the two branching processes, the lower the  $\delta^{15}\text{N}_{\text{NO}_3}$  becomes, whereas the  
143 oxygen signature is insensitive to the origin of the N in nitrification (Wankel et al. 2007).

144 The goal of this work is to improve our understanding of the N cycle in the Gulf of  
145 Aqaba, Red Sea; a system with nutrient cycles that are similar to many other seasonally stratified  
146 subtropical seas (Labiosa et al. 2003). Prior observations in the Gulf have suggested that  
147 substrate availability has a strong influence on PNM dynamics, and that nitrification and  $\text{NO}_2^-$   
148 excretion are dominant in the summer and winter respectively (Meeder et al. in prep). In this  
149 study, we seek to improve our understanding of how key physical, chemical and biological  
150 processes contribute to this seasonality and identify temporal and spatial trends in N  
151 transformation processes and rates. Our approach uses  $^{15}\text{N}$  tracer experiments together with  
152 natural abundance stable isotope measurements to quantify N transformation rates and determine  
153 the extent of N regeneration from organic matter. This combined approach characterizes  
154 different pathways in the N cycle over multiple temporal scales under both manipulated  
155 (experimental) and *in situ* conditions. Particular attention is given to processes influencing  $\text{NO}_2^-$   
156 maxima, and formation of the PNM is used as a framework to discuss the different N  
157 transformation processes occurring in the Gulf.

158

## 159 2. Materials and Methods

160

### 161 2.1 Field site

162 The Gulf of Aqaba is a seasonally stratified, subtropical water body extending from the  
163 northern Red Sea. During the summer, thermal stratification leads to oligotrophic conditions and  
164 picocyanobacteria dominate the phytoplankton community (Lindell and Post 1995; Mackey et al.  
165 2007). During the mixed winter season, mesotrophic conditions prevail, favoring eukaryotic  
166 phytoplankton (Lindell and Post 1995). A spring bloom generally occurs in March or April at the  
167 onset of stratification, in which eukaryotic phytoplankton typically dominate and are later  
168 succeeded by a secondary bloom of *Synechococcus* (Lindell and Post 1995; Mackey et al. 2009).  
169 Throughout the year the entire water column is highly oxygenated down to the sea floor.

170

### 171 2.2 In situ sampling

172 Monthly samples were collected from station A (29°28'N, 34°55'E) in the Northern Gulf  
173 of Aqaba as part of a monitoring program (<http://www.iui-eilat.ac.il/NMP>). Depth profiles were  
174 taken using a sampling CTD-Rosette (SeaBird) equipped with 12 L Niskin bottles. Depth  
175 profiles were also collected at station A before (March 18) and during (March 24 and 25) the  
176 spring bloom in 2008 as the water column transitioned from deep mixing to stratification (we  
177 refer to this as “*in situ* bloom monitoring” throughout the text).

178

### 179 2.3 <sup>15</sup>N tracer experiments

180 To quantify N transformation rates, two 1-day <sup>15</sup>N tracer experiments were conducted on  
181 back-to-back days. Surface water (1 m depth) was collected each day (during the start of the  
182 spring bloom) at ~02:00 hr from an offshore station and transported back to IUI within 1 hr.  
183 Water was dispensed into acid-washed, sample-rinsed transparent polyethylene bottles (2 L per  
184 bottle, 15 bottles per treatment). Isotopically enriched N additions were made from <sup>15</sup>N 99 atom  
185 % salts (Icon Isotopes) at the following concentrations: 0.1 μmol L<sup>-1</sup> NO<sub>3</sub><sup>-</sup>, 0.1 μmol L<sup>-1</sup> urea,  
186 0.07 μmol L<sup>-1</sup> NO<sub>2</sub><sup>-</sup>, or 0.005 μmol L<sup>-1</sup> NH<sub>4</sub><sup>+</sup>. NO<sub>3</sub><sup>-</sup> and urea were used during the 1<sup>st</sup> experiment  
187 and NO<sub>2</sub><sup>-</sup> and NH<sub>4</sub><sup>+</sup> were used in the 2<sup>nd</sup> experiment. The NO<sub>3</sub><sup>-</sup> treatment was repeated on the 2<sup>nd</sup>  
188 day, though only t<sub>0</sub> and t<sub>2</sub> time points were taken (see below for sampling schedule). Control (no  
189 addition) bottles were included in both experiments.

190

191 For each experiment, ten baseline samples were collected at ~04:00 hr prior to adding the  
192 nitrogen spikes. Spikes were administered before dawn at approximately 05:00 hr, and three  
193 bottles from each treatment were immediately sampled within 1hr of adding the spike. All  
194 remaining bottles (12 per treatment) were incubated in a flow-through tank that maintained  
195 ambient surface seawater temperature (~21°C). For each treatment, 6 bottles were incubated in  
196 the light under screening material (50% light attenuation), and 6 were incubated in the dark  
197 under a black cloth that yielded 100% light attenuation. Three light and three dark bottles were  
198 collected for each treatment at two time points. The first time point was at 12:00 hr (7 hours after  
199 the tracer was added) and the second time point was at 18:00 hr (13 hours after the tracer was  
200 added). Each time point took approximately 1 hr to process. Sub-samples were collected for flow  
201 cytometry, total and dissolved nutrients, and particulate and dissolved <sup>15</sup>N analyses as described  
202 below. Separate dedicated sets of equipment (e.g. funnels, filtration manifolds, forceps, etc) were  
203 always used for processing isotopically enriched and control samples. All equipment was acid  
washed and thoroughly rinsed with seawater prior to use.

204 Addition of  $^{15}\text{N}$  tracer to low nutrient seawater can result in increased uptake rates  
205 relative to natural levels following Michaelis-Menten kinetics. We therefore limited our tracer  
206 additions to <10% of the ambient concentrations based on measurements of surface water that  
207 were taken 1-2 days prior to the experiments. However, measurements of the actual background  
208 concentrations for  $\text{NO}_3^-$  ( $0.2 \mu\text{mol L}^{-1}$ ),  $\text{NO}_2^-$  ( $0.03 \mu\text{mol L}^{-1}$ ),  $\text{NH}_4^+$  ( $0.025 \mu\text{mol L}^{-1}$ ) were lower  
209 during the experiment than expected. Our measured rates may therefore overestimate the actual  
210 rates by 50%, 230%, and 20% for  $\text{NO}_3$ ,  $\text{NO}_2^-$ , and  $\text{NH}_4^+$ , respectively based on Michaelis-  
211 Menten kinetics (Dugdale and Goering 1967). Urea concentrations were assumed to be 10% of  
212 DON, typical of oligotrophic surface waters (Jackson and Williams 1985; Eppley et al. 1977)  
213 and consistent with prior measurements for urea in the Gulf of Aqaba (A. Post, unpublished  
214 data). Our measured urea transformation rates could therefore underestimate the actual rates by a  
215 maximum of 90% if all DON was urea, however this is highly unlikely.

216 Despite the potentially large over or under estimates reported above we note that the rates  
217 calculated should still be within a typical range of values for the Gulf during this time of year  
218 because the  $^{15}\text{N}$  additions were based on real concentration levels measured within a few days of  
219 the experiment and the phytoplankton composition and abundance did not change significantly  
220 over that time (data not shown).

221

#### 222 **2.4 Particulate nitrogen $^{15}\text{N}$ analysis**

223 Samples for particulate N concentration and isotopic composition were collected for the  
224 *in situ* bloom monitoring and for the  $^{15}\text{N}$  tracer experiment. Samples were obtained by filtering 1  
225 L aliquots of sample water through pre-combusted ( $500^\circ\text{C}$ , 5 hr) 25mm glass fiber filters (GF/F,  
226 Whatman). Sample filters were analyzed at the Stable Isotope Facility at University of  
227 California, Davis using a PDZ Europa ANCA-GSL elemental analyzer interfaced to a PDZ  
228 Europa 20-20 isotope ratio mass spectrometer (IRMS, Sercon Ltd., Cheshire, UK). Sample  $\delta^{15}\text{N}$   
229 values were calculated by adjusting the measured values using an empirical calibration scale  
230 based on laboratory standards. Two laboratory standards (NIST 1547 and acetanilide) were  
231 analyzed every 12 samples. Laboratory standards were calibrated against NIST Standard  
232 Reference Materials (IAEA-N1, IAEA-N2, IAEA-N3, IAEA-CH7, and NBS-22). The standard  
233 deviation of repeated measurements for the method is 0.2‰.

234

#### 235 **2.5 $\delta^{15}\text{N}$ of dissolved inorganic nitrogen**

236 Water samples for dissolved  $\text{NO}_3^-$  and  $\text{NO}_2^-$  (N+N) isotopic composition were collected  
237 during the *in situ* bloom monitoring and during the  $^{15}\text{N}$  tracer experiment. Samples were filtered  
238 through pre-combusted (500°C, 5h) glass fiber filters (GF/F, Whatman) by hand under low  
239 pressure using a syringe and Swinnex filter holder. Filtrate was immediately acidified to <pH 3  
240 with trace metal grade hydrochloric acid and stored in the dark at room temperature until  
241 analysis. The  $\delta^{15}\text{N}$  and  $\delta^{18}\text{O}$  were determined using the method of McIlvin and Altabet (2005).  
242 Briefly, the samples were rendered alkaline by addition of excess MgO, and  $\text{NO}_3^-$  was reduced to  
243  $\text{NO}_2^-$  by shaking overnight with activated cadmium (Cd).  $\text{NO}_2^-$  was then reduced to nitrous oxide  
244 with sodium azide in an acetic acid buffer for one hour, followed by neutralization with sodium  
245 hydroxide and analysis on a continuous flow isotope ratio mass spectrometer (IRMS). Data  
246 obtained by this method include contribution from  $\text{NO}_3^-$  and  $\text{NO}_2^-$ , which we refer to in the text  
247 as N+N for simplicity. The isotopic composition of  $\text{NO}_2^-$  alone was determined in the  $^{15}\text{N}$  tracer  
248 experiment samples by omitting the  $\text{NO}_3^-$  reduction step.

249 All samples were calibrated and blank corrected using the international isotopic standards  
250 USGS 32, USGS 34, and USGS 35 for  $\text{NO}_3^-$  and three in house standards for  $\text{NO}_2^-$ . The  
251 reference scale for N and O isotopic composition were atmospheric  $\text{N}_2$  and SMOW (standard  
252 mean ocean water), respectively. Standards were run before, after, and at 12-15 sample intervals  
253 during the run. Analytical precision measured from multiple determinations on standards was  
254 0.2‰ for  $\delta^{15}\text{N}$  and 0.7‰ for  $\delta^{18}\text{O}$ . The detection limit for successful isotopic determination was  
255 ~2 nmol N (corresponding to ~130 nmol  $\text{N L}^{-1}$  based on the volumes of sample we used). For  
256 samples falling below this concentration threshold in the  $^{15}\text{N}$  tracer experiment, it was possible to  
257 increase the N concentration by addition of a known quantity of standard  $\text{NO}_2^-$  material because  
258 introduction of even a small fraction of  $^{15}\text{N}$  tracer into the  $\text{NO}_2^-$  pool would measurably affect the  
259 isotopic composition of the mixture. This allowed us to calculate the isotopic composition of the  
260 sample from the measured composition of the mixture and the known composition of the  
261 standard based on conservation of mass. This process could not be used for natural abundance  
262 samples collected during the spring bloom because the isotope signals of the sample and the  
263 standards were too similar to determine an accurate value. Therefore, only the isotopic  
264 composition of the combined N+N was determined for those samples.

265 Since  $\text{NO}_2^-$  was not removed, the Cd reduction method measured the combined isotope  
266 composition of  $\text{NO}_3^-$  and  $\text{NO}_2^-$  in our samples, and the isotopic values of samples containing a  
267 high proportion of  $\text{NO}_2^-$  will therefore be affected by an analytical artifact. To get a conservative  
268 estimate of what the values of  $\delta^{15}\text{N}_{\text{NO}_3}$  and  $\delta^{18}\text{O}_{\text{NO}_3}$  would be without the  $\text{NO}_2^-$  signal, two  
269 corrections were applied. For O, we assumed that all of the O atoms in  $\text{NO}_2^-$  exchanged with the  
270 seawater for which the abiotic equilibrium isotope effect causes the O in  $\text{NO}_2^-$  to become  
271 isotopically enriched by 14‰ relative to the surrounding water (Casciotti 2007). This assumption  
272 is valid as samples were acidified immediately after collection and equilibration of oxygen atoms  
273 between water and nitrite is rapid at low pH (McIlvin and Casciotti, 2007). This would lead to  
274  $\delta^{18}\text{O}$  values in  $\text{NO}_2^-$  of ~15.5-16.5‰ for the Gulf of Aqaba, where the  $\delta^{18}\text{O}$  of water is 1.5-  
275 2.5‰. We then used conservation of mass to determine what the  $\delta^{18}\text{O}$  would be if no  $\text{NO}_2^-$  was  
276 present by subtracting out its signal using the  $\text{NO}_2^-$  concentration data. Similarly for N, we  
277 calculated what the  $\delta^{15}\text{N}$  would be if no  $\text{NO}_2^-$  was present by assuming all of the  $\text{NO}_2^-$  in the  
278 sample was 12.8 ‰ lighter than  $\text{NO}_3^-$  due to the inverse fractionation effect associated with nitrite  
279 oxidation (Casciotti et al. 2010). While nitrification is not necessarily the dominant process  
280 throughout the water column, it is likely to be an important process where  $\text{NO}_2^-$  levels are high,  
281 so this assumption provides a conservative yet realistic correction. The  $\delta^{15}\text{N}$  of the combined



282 N+N pool may therefore be lighter than expected for  $\text{NO}_3^-$  alone. The influence of these  
 283 processes is dependent on the portion  $\text{NO}_2^-$  in the N+N pool.  $\text{NO}_2^-$  comprised up to 21% of the  
 284 N+N in some surface samples from the March 24 and 25 profiles; and the specific implications  
 285 of this on our data are discussed along with the results. We note that a number of methods are  
 286 now available to remove  $\text{NO}_2^-$  from samples prior to analysis (Granger and Sigman 2009) such  
 287 that the  $\delta^{15}\text{N}$  of  $\text{NO}_3^-$  can be measured via the Cd reduction method without this analytical  
 288 artifact.

289

## 290 **2.6 N uptake and transformation rate calculations**

291 N uptake rates were determined from particulate N samples collected at the beginning  
 292 and end of the  $^{15}\text{N}$  tracer experiment. Uptake rates ( $\rho$ ) were measured for  $\text{NO}_3^-$ ,  $\text{NO}_2^-$ ,  $\text{NH}_4^+$  and  
 293 urea using two equations based on a constant uptake model (Dugdale and Wilkerson 1986):  
 294

$$295 \quad \rho_t = \frac{c_t}{t} \times \frac{{}^{15}\text{N}_s - \langle F \rangle}{{}^{15}\text{N}_{\text{enr}} - \langle F \rangle} \quad (1)$$

296

$$297 \quad \rho_0 = \frac{c_0}{t} \times \frac{{}^{15}\text{N}_s - \langle F \rangle}{{}^{15}\text{N}_{\text{enr}} - {}^{15}\text{N}_s} \quad (2)$$

298 Where  ${}^{15}\text{N}_s$  is the atom%  $^{15}\text{N}$  in the sample measured by a mass spectrometer as  
 299 described above;  ${}^{15}\text{N}_{\text{enr}}$  is the atom%  $^{15}\text{N}$  in the initially labeled pool of  $\text{NO}_3^-$ ,  $\text{NO}_2^-$ ,  $\text{NH}_4^+$  or  
 300 Urea;  $\langle F \rangle$  is the natural abundance of  $^{15}\text{N}$  (in atom%); and  $t$  is the incubation time. The  
 301 quantities  $c_t$  and  $c_0$  denote the particulate N concentration ( $\mu\text{mol L}^{-1}$ ) at time  $t$  and time zero  
 302 respectively, and are used to calculate the absolute uptake rate, with units mass per volume per  
 303 time ( $\text{nmol N L}^{-1} \text{ day}^{-1}$ ). Equation 1 can underestimate and equation 2 can overestimate the actual  
 304 uptake rate if there is a significant change in the amount of particulate matter over the course of  
 305 the experiment (Dugdale and Wilkerson 1986). This effect is small for low uptake rates but can  
 306 increase as uptake rates increase. We found that values from these equations agreed well for all  
 307 but our two highest uptake rates. We therefore report an average of  $\rho_t$  and  $\rho_0$  as suggested by  
 308 Dugdale and Wilkerson (1986).

309 Rates of  $\text{NH}_4^+$  oxidation and combined urea mineralization and subsequent oxidation of  
 310 the  $\text{NH}_4^+$  generated were determined from the isotopic composition of  $\text{NO}_2^-$  measured at the 1 hr  
 311 time point in the  $^{15}\text{N}$  tracer experiment using the following equation:

$$312 \quad r = \frac{1}{t} \times \frac{{}^{15}\text{N}_t c_t - \langle F_{\text{NO}_2} \rangle c_0}{{}^{15}\text{N}_{\text{enr}} - \langle F_{\text{NO}_2} \rangle} \quad (5)$$

313 Where  $r$  is the net reaction rate,  ${}^{15}\text{N}_t$  is the atom%  $^{15}\text{N}$  in the sample  $\text{NO}_2^-$  measured by mass  
 314 spectrometer as described above for the first time point;  ${}^{15}\text{N}_{\text{enr}}$  is the atom%  $^{15}\text{N}$  in the initially  
 315 labeled pool of  $\text{NH}_4^+$  or Urea;  $\langle F_{\text{NO}_2} \rangle$  is the natural abundance of  $^{15}\text{N}$  of  $\text{NO}_2^-$  in the baseline  
 316 sample water (in atom%); and  $t$  is the incubation time. The quantities  $c_t$  and  $c_0$  denote the  $\text{NO}_2^-$   
 317 concentration ( $\mu\text{mol L}^{-1}$ ) at time  $t$  and time zero (before additions were made), respectively.

318 Determination of rates based on enrichment experiments is based on the assumption that  
 319 the labeled fraction represents a constant portion of the total substrate pool throughout the  
 320 experiment. For example, if  $^{15}\text{NO}_3^-$  tracer is added as 10% of the background  $\text{NO}_3^-$  concentration  
 321 at the start of the experiment, then the atomic percent of  $^{15}\text{NO}_3^-$  should ideally remain 10%  
 322 throughout the experiment for accurate measurements to be made. Transformation rates can then

323 be calculated based on this relationship once the amount of label that gets transformed is  
324 measured (e.g. for every one  $^{15}\text{N}$  atom taken up, 9  $^{14}\text{N}$  atoms also get taken up). These estimates  
325 are subject to error if rapid substrate regeneration occurs (Gilbert et al. 1982; Dugdale and  
326 Wilkerson 1986). For example, if  $\text{NO}_3^-$  is regenerated during an experiment, then the labeled  
327 fraction will continually get “diluted” over the course of the experiment. This effect becomes  
328 more pronounced in longer experiments. We were unable to quantify dissolved N  
329 transformations based on the 7 and 13 hour time points in the  $^{15}\text{N}$  tracer experiment because the  
330 turnover rates were more rapid than we expected and dilution of the isotope label occurred, thus  
331 we use the 1 hour point only.

332

## 333 **2.7 Total and Dissolved Nutrients, chl *a* and Irradiance**

334 Total N,  $\text{NO}_3^-$  and  $\text{NO}_2^-$  concentrations were collected during all *in situ* monitoring, as  
335 well as during the nutrient addition experiment and  $^{15}\text{N}$  tracer experiment. Concentrations of  
336  $\text{NO}_3^-$  and  $\text{NO}_2^-$  were determined using colorimetric methods described by Hansen and Koroleff  
337 (1999) modified for a Flow Injection Autoanalyzer (FIA, Lachat Instruments Model QuickChem  
338 8000) as described previously (Mackey et al. 2007). The precision of the methods was  $0.05 \mu\text{mol}$   
339  $\text{L}^{-1}$  for  $\text{NO}_2^-$  and  $\text{NO}_3^-$ . The detection limit for these nutrients was  $0.02 \mu\text{mol L}^{-1}$ . Ammonium  
340 samples from *in situ* field samples collected during the spring bloom progression were measured  
341 using the ortho-phthaldehyde method described by Holmes et al. (1999) with a precision of  $0.02$   
342  $\mu\text{mol L}^{-1}$  and a detection limit of  $0.01 \mu\text{mol L}^{-1}$ . Total N was determined for March 24 and 25  
343 and for the  $^{15}\text{N}$  tracer experiment on whole water samples without filtration. Samples were  
344 digested by persulfate oxidation, reduced in a copper-cadmium column, and analyzed  
345 colorimetrically following D’Elia et al (1977). The detection limit was  $1.4 \mu\text{mol L}^{-1}$ . Dissolved  
346 organic N (DON) was calculated by subtracting the particulate N and total inorganic N ( $\text{NO}_3^- +$   
347  $\text{NO}_2^- + \text{NH}_4^+$ ) from total N. Photosynthetically available radiation (PAR, 400-700 nm) was  
348 measured using a standard high-resolution profiling reflectance radiometer (Biospherical PRR-  
349 800, data courtesy D. Iluz). Chl *a* was measured fluorometrically using a Turner Fluorometer  
350 (Turner Designs 10-AU-005-CE) following 90% acetone extraction at  $0^\circ\text{C}$  for 24 hr as described  
351 previously (Mackey et al. 2009).

352

## 353 **2.8 Flow cytometry**

354 Flow cytometry was used to determine the abundance of phytoplankton and non-  
355 photosynthetic microbes in samples from *in situ* bloom monitoring, the nutrient addition  
356 experiment, and the  $^{15}\text{N}$  tracer experiment. Samples were preserved with 0.1% glutaraldehyde,  
357 flash frozen in liquid nitrogen, and stored at  $-80^\circ\text{C}$  until analysis. Cell abundances in samples  
358 from the *in situ* bloom monitoring and the  $^{15}\text{N}$  tracer experiment were measured using a LSRII  
359 cell analyzer (Becton Dickinson Immunocytometry Systems, San Jose, CA). Before analysis  
360 SYTO 42 blue fluorescent nucleic acid stain (Invitrogen, Molecular Probes) was added at a final  
361 concentration of  $8 \mu\text{mol L}^{-1}$  and samples were incubated at room temperature for 5 minutes. The  
362 SYTO 42 stain has excitation and emission peaks at 433 nm and 460 nm respectively, and offers  
363 strong fluorescence enhancement upon binding nucleic acids such that the fluorescence signal  
364 from stained cells is maximized relative to background. Cell populations were identified using  
365  $90^\circ$  light scatter, autofluorescence of photopigments, and SYTO 42 fluorescence. Chlorophyll  
366 positive (phytoplankton) cells were identified as *Synechococcus* based on positive phycoerythrin  
367 content. *Prochlorococcus*, picoeukaryotes (eukaryotic phytoplankton  $<2 \mu\text{m}$  in diameter) and  
368 nanophytoplankton (phytoplankton  $>2 \mu\text{m}$  in diameter) were identified based on their relative

369 scatter and chlorophyll fluorescence levels. Non-photosynthetic cells were identified based on  
370 lack of chlorophyll fluorescence and positive SYTO 42 staining. Cell numbers were determined  
371 by spiking each sample with a known concentration of 1µm fluorescent yellow green calibration  
372 beads (Polysciences).

373

### 374 3. Results

375

#### 376 3.1 *In situ* monthly monitoring

377 Time series analyses of  $\text{NO}_3^-$  and  $\text{NO}_2^-$  depth profiles over representative one-year  
378 periods showed a clear relationship with seasonal mixing and stratification (**Fig. 2**). In February  
379 2008 the water column was mixed down to the seafloor before stratification occurred in March  
380 (**Fig. 1A**). In the winter (e.g. January-March),  $\text{NO}_3^-$  and  $\text{NO}_2^-$  levels were inversely related, with  
381 higher  $\text{NO}_2^-$  levels in the upper mixed layer than at depth. Primary  $\text{NO}_2^-$  maxima (PNM) began  
382 to take shape in March or April, which is the spring season when the water column first begins to  
383 stratify. In the summer (e.g. May-September), when the euphotic depth is approximately 100 m,  
384 PNM in the stratified water column were evident between 50-200 m.  $\text{NO}_3^-$  concentrations  
385 remained below detection throughout the euphotic zone, and increased gradually with depth  
386 below 100 m. This trend is typical of other years, although the actual  $\text{NO}_3^-$  and  $\text{NO}_2^-$   
387 concentrations within and below the mixed layer vary with mixing depth. For example in 2003,  
388 when the mixing depth was only down to ~400 m,  $\text{NO}_3^-$  and  $\text{NO}_2^-$  concentrations differed from  
389 those in 2008, but still retained their inverse relationship in the winter and PNM formation the  
390 summer (**Fig. 2B**).

391 Monthly monitoring of chl *a* also showed seasonal changes (**Fig. 2**), with homogenous  
392 mixed layer profiles in the winter months and the formation of deep chlorophyll maxima (DCM)  
393 between 50-100 m in the stratified summer months. The PNM was located at or below the depth  
394 of the DCM in 2008 and 2003.

395

#### 396 3.2 *In situ* spring bloom monitoring

397 To determine how changing physical, chemical, and biological water column  
398 characteristics influence N transformation rates, we compared nutrient, chlorophyll *a*, flow  
399 cytometry, and isotope data from 3 profiles taken during early stages of stratification in 2008.  
400 The first profile was taken when the water column retained many of its characteristics from  
401 previous deep mixing. The other profiles were taken on two consecutive days after stratification  
402 was established. Prior to the spring bloom in 2008, mixing depths extending to greater than 600  
403 m as judged from nutrient (**Fig. 3A**) and density profiles (not shown).

##### 404 3.2.1 *Nutrients*

405 Field sampling conducted on March 18 at the very onset of stratification (**Fig. 3A**)  
406 showed nearly homogenous  $\text{NO}_3^-$  levels ( $\sim 3 \mu\text{mol L}^{-1}$ ) throughout the water column, with a  
407 tendency towards lower concentrations in surface waters ( $\sim 2 \mu\text{mol L}^{-1}$ ). In surface waters,  $\text{NO}_2^-$   
408 was higher ( $0.23 \mu\text{mol L}^{-1}$ ) than throughout the rest of the euphotic zone ( $\sim 0.18 \mu\text{mol L}^{-1}$ ),  
409 whereas  $\text{NH}_4^+$  levels peaked at 100 m ( $0.42 \mu\text{mol L}^{-1}$ ). Sampling conducted on 24 and 25 March  
410 2008 (**Fig. 3A**) following stratification and during the spring bloom showed continued  
411 drawdown of  $\text{NO}_3^-$  in surface waters, as well as the formation of a PNM peak between 200-250  
412 m (reaching  $0.59 \mu\text{mol L}^{-1}$  at 200 m on 25 March). Maximum  $\text{NH}_4^+$  levels occurred above the  
413  $\text{NO}_2^-$  maxima at depths of 160-200 m, and reached  $0.59 \mu\text{mol L}^{-1}$  at 200 m on 24 March.  
414 Particulate N levels increased in surface waters from 0.43 to  $2.57 \mu\text{mol N L}^{-1}$  between March 18-

415 24, and decreased to  $1.08 \mu\text{mol N L}^{-1}$  by March 25 (**Fig. 3B**). Total N was  $12.1 \pm 0.7 \mu\text{mol N L}^{-1}$   
416 ( $n=21$ ) for all depths in the water column (**Fig. 3C**).

### 417 **3.2.2 Phytoplankton growth**

418 Chl *a* profiles from 18, 24, and 25 March 2008 (**Fig. 3A**) showed the progression of the  
419 phytoplankton bloom following stratification. On March 18, the chl *a* profile was homogenous  
420 throughout the euphotic zone ( $\sim 0.2 \text{ mg m}^{-3}$ ), except in the upper 20 m where it increased to  $\sim 0.5$   
421  $\text{mg m}^{-3}$  (**Fig. 3A**). Chl *a* maxima were apparent in both the 24 and 25 March profiles, reaching  
422 maximum concentrations of  $0.8\text{-}0.9 \text{ mg m}^{-3}$  between 40-60 m.

423 Flow cytometry measurements show that by March 24 and 25, phytoplankton populations  
424 were most abundant in the upper water column and were dominated by *Synechococcus* and  
425 nanophytoplankton (**Fig. 4**). Picoeukaryotes were present in smaller numbers (**Fig. 4**), and no  
426 substantial populations of *Prochlorococcus* were identified (data not shown). In the surface,  
427 *Synechococcus* reached  $\sim 8.0 \times 10^4 \text{ cells mL}^{-1}$  and nanophytoplankton reached  $\sim 2.0 \times 10^4 \text{ c mL}^{-1}$ . Both  
428 populations increased approximately two-fold between March 24 and 25 between depths of 60-  
429 120 m despite being below the 1% light level (60 m). The picoeukaryote population decreased  
430 from  $\sim 3 \times 10^3$  to  $\sim 0.8 \times 10^3 \text{ c mL}^{-1}$  between March 24-25 in surface waters. Non-photosynthetic cells  
431 ranged from  $5.00 \times 10^5$ - $2.00 \times 10^6 \text{ c mL}^{-1}$  throughout the water column (**Fig. 4**).

### 432 **3.2.3 Isotopes of dissolved N+N and particulate N**

433 Prior to stratification on March 18<sup>th</sup> the  $\delta^{15}\text{N}_{\text{N+N}}$  and  $\delta^{18}\text{O}_{\text{N+N}}$  were homogenous through  
434 the water column, averaging  $2.6 \pm 0.08 \text{ ‰}$  and  $6.7 \pm 0.17 \text{ ‰}$ , respectively (**Fig. 5A,B**). These  
435 values are distinctly different from those expected for average open ocean deep water nitrate  
436  $\delta^{15}\text{N}$  (5 ‰; Sigman et al. 2000) and  $\delta^{18}\text{O}$  (2 ‰; Knapp et al. 2008). As stratification progressed  
437 and the bloom developed,  $\delta^{15}\text{N}_{\text{N+N}}$  and  $\delta^{18}\text{O}_{\text{N+N}}$  values both increased in surface waters.  $\delta^{15}\text{N}_{\text{N+N}}$   
438 reached peak values of  $\sim 10 \text{ ‰}$  at 60 and 20 m on March 24 and 25 respectively (**Fig. 5A**),  
439 whereas maximum  $\delta^{18}\text{O}_{\text{N+N}}$  values of 53 and 40 ‰ were seen at the surface (**Fig. 5B**). The  $\delta^{15}\text{N}$   
440 also showed a subsurface peak of  $\sim 11 \text{ ‰}$  at 160 m. These values of  $\delta^{15}\text{N}_{\text{N+N}}$  and  $\delta^{18}\text{O}_{\text{N+N}}$  include  
441 an influence from  $\text{NO}_2^-$ , and may therefore differ from values that would be expected from  $\text{NO}_3^-$   
442 alone. As outlined above, an isotope mass balance calculation was used to correct for this  
443 artifact, the corrected data are plotted in **Fig. 5A and B** along with the actual measured data. The  
444 difference between measured and corrected values is greatest for depths in the vicinity of the  
445 PNM, and is greater for  $\delta^{15}\text{N}_{\text{N+N}}$  than for  $\delta^{18}\text{O}_{\text{N+N}}$ . Despite this limitation, trends in vertical and  
446 temporal distributions are larger than can be explained by this artifact alone, hence showing true  
447 variability.

448 The dual isotope plot of  $\delta^{18}\text{O}_{\text{N+N}}$  and  $\delta^{15}\text{N}_{\text{N+N}}$  (**Fig. 6**) shows the tight clustering of values  
449 on March 18 as a result of the values being homogenous throughout the water column. If nitrate  
450 assimilation was the only process impacting the nitrate pool as stratification progressed, we  
451 would expect to see the values sit along a 1:1 line as isotopic fractionation during nitrate  
452 assimilation is known to produce a 1:1 increase in the  $\delta^{15}\text{N}$  and  $\delta^{18}\text{O}$  of nitrate (Granger et al,  
453 2004). Instead by March 25 the ratios were close to 5:1 (**Fig. 6C**), suggesting a decoupling of the  
454 N and O isotopes of nitrate and thus the importance of other processes in addition to nitrate  
455 assimilation. We note that the slopes of the  $\delta^{18}\text{O}_{\text{N+N}} : \delta^{15}\text{N}_{\text{N+N}}$  line measured here could be high  
456 due to the analytical artifact contributed by  $\text{NO}_2^-$  in some samples as discussed above. However,  
457 although the value of the slopes were not as high overall for any given day in the corrected data  
458 set **Fig. 6** (gray circles), the increase in the slopes between days is still apparent.

459 The  $\delta^{15}\text{N}$  values of particulate matter on March 18 averaged  $-4.7\text{‰}$  (**Fig. 5C**). Values  
460 increased as stratification was established. Within the upper 100 m, values ranged from  $0.8\text{‰}$  to  
461  $6.4\text{‰}$ , and increased with depth, reaching nearly  $20\text{‰}$  at 600m.

462

### 463 **3.3 $^{15}\text{N}$ tracer experiment**

464 At the start of the  $^{15}\text{N}$  tracer experiment the phytoplankton population was dominated by  
465 *Synechococcus* ( $1.24 \times 10^5 \text{ c mL}^{-1}$ ), followed by nanophytoplankton ( $4.66 \times 10^4 \text{ c mL}^{-1}$ ) and  
466 picoeukaryotes ( $4.2 \times 10^3 \text{ c mL}^{-1}$ ). Non-photosynthetic cells were approximately an order of  
467 magnitude more abundant than phytoplankton ( $\sim 1.4 \times 10^6 \text{ c mL}^{-1}$ ). There were no appreciable  
468 changes in the community composition of the water used on the 1<sup>st</sup> and 2<sup>nd</sup> day of the experiment  
469 (not shown).

470 In order to estimate fluxes of N between different N pools, we used isotope data from the  
471  $^{15}\text{N}$  tracer experiment along with nutrient inventory mass balance. We sought to quantify rates  
472 for the following N transformations: (1) biological assimilation for  $\text{NO}_3^-$ ,  $\text{NO}_2^-$ ,  $\text{NH}_4^+$ , and urea;  
473 (2) oxidation of  $\text{NH}_4^+$  and urea (via  $\text{NH}_4^+$  intermediate) to  $\text{NO}_2^-$  during nitrification; and (3)  
474 incomplete  $\text{NO}_3^-$  reduction to  $\text{NO}_2^-$  by phytoplankton. The rate of N transfer between two pools  
475 can be estimated from tracer experiments if dilution of the  $^{15}\text{N}$  label by substrate regeneration is  
476 minimal during the experiment, as described above. Dilution of the isotope spike during  
477 substrate regeneration generates artificially low rate estimates because the ratio of tracer to  
478 unlabeled N becomes smaller than assumed based on initial concentrations of the substrate (i.e.,  
479 the regenerated substrate “dilutes” the tracer as the experiment progresses). Rates will also be  
480 underestimated if the N product formed from the tracer is rapidly consumed by another process.  
481 These sources of error can be minimized by selecting appropriate time scales over which to  
482 calculate different rates (Gilbert et al. 1982), and these concerns are discussed for each rate  
483 estimate below.

484

### 485 **3.4 Biological N assimilation**

486 N uptake and assimilation rates were estimated in the  $^{15}\text{N}$  tracer experiment based on  
487 direct measurements of enrichment in the particulate matter for both light and dark treatments.  
488 Error from dilution of the  $^{15}\text{N}$  label due to substrate regeneration increases with longer  
489 incubation times, as does the likelihood that phytoplankton will excrete and re-assimilate the  
490 tracer (Gilbert et al. 1982; Bronk et al. 1994). However, assimilation rates immediately following  
491 tracer addition are generally higher than actual *in situ* rates, a problem that can be ameliorated by  
492 using a slightly longer incubation time. We used the 1, 7 and 13 hr time points to calculate  
493 uptake rates; however, our calculated values could underestimate the actual assimilation rates by  
494 a factor of 2 due to dilution of the  $^{15}\text{N}$  label from regeneration of substrate (Gilbert et al. 1982),  
495 and by 50-74% due to excretion of the  $^{15}\text{N}$  label as DON following uptake (Bronk et al. 1994).  
496 The background urea concentration during the experiment was  $1.0 \pm 0.1 \mu\text{mol L}^{-1}$ . Urea uptake  
497 ( $1194 \text{ nmol N L}^{-1} \text{ day}$ ) was approximately three-fold faster than  $\text{NO}_3^-$  uptake ( $\sim 434 \text{ nmol N L}^{-1}$   
498  $\text{day}$ ) in the light (**Table 1, Fig. 7A,B**). Both urea and  $\text{NO}_3^-$  uptake rates were higher in light  
499 bottles than in dark bottles ( $476 \text{ nmol N L}^{-1} \text{ day}$  for urea and  $58 \text{ nmol N L}^{-1} \text{ day}$  for  $\text{NO}_3^-$ , **Table**  
500 **1, Fig. 7A,B**). For the  $\text{NH}_4^+$  treatment, all of the  $^{15}\text{NH}_4^+$  spike was assimilated prior to the 7 hr  
501 sampling in both light and dark bottles, so we only report uptake values based on the 1 hr time  
502 point ( $314 \text{ nmol L}^{-1} \text{ day}^{-1}$ , **Table 1**). For  $\text{NO}_2^-$ , all of the  $^{15}\text{NO}_2^-$  was assimilated before the 13 hr  
503 sampling; however, based on the 7 hr time point when  $^{15}\text{N}$  was still available  $\text{NO}_2^-$  uptake was  
504 three-fold higher in the light ( $94 \text{ nmol N L}^{-1} \text{ day}$ ) than in the dark ( $29 \text{ nmol N L}^{-1} \text{ day}$ ) (**Table 1**).

505 N uptake rates at 50% surface PAR were higher for  $\text{NO}_3^-$  ( $\sim 420 \text{ nmol L}^{-1} \text{ day}^{-1}$ ) than for  
506  $\text{NO}_2^-$  ( $94 \text{ nmol L}^{-1} \text{ day}^{-1}$ ; Table 1). As mentioned above,  $\text{NO}_2^-$  uptake rates could have been  
507 underestimated by 2 fold in the  $^{15}\text{N}$  addition experiment; however, even accounting for this  
508 potential error,  $\text{NO}_3^-$  uptake still exceeded  $\text{NO}_2^-$  uptake. We note that the uptake rates could be  
509 more similar when  $\text{NO}_2^-$  concentrations are higher.

510

### 511 **3.5 Oxidation of $\text{NH}_4^+$ and urea to $\text{NO}_2^-$**

512 Oxidation rates of  $\text{NH}_4^+$  and urea (following mineralization to  $\text{NH}_4^+$ ) were determined  
513 based on measurements of  $\text{NO}_2^-$  isotopic composition after  $^{15}\text{N}$  enriched spikes of  $\text{NH}_4^+$  or urea  
514 were added in the  $^{15}\text{N}$  tracer experiment. We calculated rates for the 1hr time point, but were  
515 unable to quantify rates from the 7 and 13 hr time points because the  $^{15}\text{N}$  enrichments were too  
516 small or the turnover of the N pools was too rapid for accurate estimates to be made over these  
517 longer time scale (substrate regeneration affected the results). Oxidation of  $\text{NH}_4^+$  to  $\text{NO}_2^-$   
518 occurred at a rate of  $16.4 \pm 8.1 \text{ nmol N L}^{-1} \text{ d}^{-1}$  (or  $0.68 \pm 0.34 \text{ nmol N L}^{-1} \text{ hr}^{-1}$ ). Mineralization of  
519 urea to  $\text{NH}_4^+$  with subsequent oxidation to  $\text{NO}_2^-$  occurred at a rate of  $14.1 \pm 7.6 \text{ nmol N L}^{-1} \text{ d}^{-1}$   
520 ( $0.59 \pm 0.32 \text{ nmol N L}^{-1} \text{ hr}^{-1}$ ; **Table 1**).

521

### 522 **3.6 Reduction of $\text{NO}_3^-$ to $\text{NO}_2^-$**

523 We were unable to measure reduction of  $\text{NO}_3^-$  to  $\text{NO}_2^-$  based on data from the  $^{15}\text{N}$  tracer  
524 experiment. For the 7 and 13 hr time points, substrate regeneration caused dilution of the  $^{15}\text{N}$   
525 label during the experiment and precluded accurate calculations from being made. In addition,  
526 since reduction of  $\text{NO}_3^-$  to  $\text{NO}_2^-$  is driven by light, we were unable to measure this process in  
527 samples from the 1 hr time point, because the samples were collected before dawn and received  
528 no light to initiate this process. Therefore, the rate of  $\text{NO}_3^-$  reduction based on the 1 hr time point  
529 in the  $^{15}\text{N}$  tracer experiment was negligible, as expected.

530 However, incomplete reduction of  $\text{NO}_3^-$  and release of  $\text{NO}_2^-$  by light limited  
531 phytoplankton is a well documented phenomenon in both field and culture studies (Collos 1998;  
532 Lomas and Lipschultz 2006 and references therein). The rate of  $\text{NO}_3^-$  reduction to  $\text{NO}_2^-$  by  
533 phytoplankton is dependent on light and on phytoplankton abundance. Therefore, if  
534 phytoplankton were a significant source of  $\text{NO}_2^-$  in a certain portion of the water column  
535 following stratification, then we would expect the change in  $\text{NO}_2^-$  concentration to be correlated  
536 with both light and chlorophyll abundance over those depths. We therefore calculated a range of  
537 net  $\text{NO}_2^-$  formation rates based on changes in the *in situ*  $\text{NO}_2^-$  concentrations measured during  
538 the spring bloom between March 18-24, and tested if they were correlated with irradiance or chl  
539 *a* concentrations. These  $\text{NO}_2^-$  formation rates are “net accumulation” rates, and represent the  
540 combined input from all  $\text{NO}_2^-$  sources (e.g. phytoplankton or  $\text{NH}_4^+$  oxidation) as well as all  $\text{NO}_2^-$   
541 sinks (e.g. assimilation or  $\text{NO}_2^-$  oxidation). While all of these processes can potentially influence  
542 the calculated rate at each depth, light and chlorophyll abundance will correlate most strongly  
543 with  $\text{NO}_2^-$  formation over depths where incomplete reduction of  $\text{NO}_3^-$  and expulsion of  $\text{NO}_2^-$  by  
544 light limited phytoplankton is the dominant process.

545 We found that net  $\text{NO}_2^-$  formation was strongly correlated with light between 60-200 m  
546 ( $R^2=0.99$ , **Fig. 8B**, **Table 2**) and ranged from  $2.2\text{-}58 \text{ nmol L}^{-1} \text{ day}^{-1}$  ( $0.092\text{-}2.4 \text{ nmol L}^{-1} \text{ hr}^{-1}$ ). Chl  
547 *a* concentration was also correlated with  $\text{NO}_2^-$  formation rates; however, this relationship was  
548 primarily because chl *a* abundance is also controlled by light (**Fig. 8C**). To parse the independent  
549 effect of chl *a* concentration on  $\text{NO}_2^-$  formation rate, we compared the residual chl *a* and  $\text{NO}_2^-$   
550 formation rate data after subtracting out the influence of light on each parameter according to the

551 following procedure.

552 The influence of light on each parameter (chl *a* concentration or NO<sub>2</sub><sup>-</sup> formation rate) was  
553 calculated based on the equations best fit as shown in **Fig. 8B** and **C**. The calculated value was  
554 subtracted from the actual measured value to obtain the residual value. The residual values are  
555 the portions of the actual chl *a* and net NO<sub>2</sub><sup>-</sup> formation rate measurements that are not accounted  
556 for by light. The residual values of chl *a* and net NO<sub>2</sub><sup>-</sup> formation rate were then plotted (**Fig. 8D**)  
557 to determine the relationship between chl *a* and net NO<sub>2</sub><sup>-</sup> formation rate. With the exception of  
558 one outlier point (showing a lower NO<sub>2</sub><sup>-</sup> formation rate than expected), a strong linear  
559 relationship existed between residual chl *a* levels and residual NO<sub>2</sub><sup>-</sup> formation rates (**Fig. 8D**).  
560 Interestingly, the outlier point coincided with an NH<sub>4</sub><sup>+</sup> peak at 120 m that got consumed between  
561 March 18 and 24 (**Fig. 3A**). The NO<sub>2</sub><sup>-</sup> formation rate at this depth did not correspond to chl *a*  
562 because a larger portion of the NO<sub>2</sub><sup>-</sup> at that depth was likely formed by NH<sub>4</sub><sup>+</sup> oxidation. If all of  
563 the NH<sub>4</sub><sup>+</sup> drawn down at this depth between March 18-24 was oxidized to NO<sub>2</sub><sup>-</sup> it would have  
564 contributed ~115 nmol NO<sub>2</sub><sup>-</sup> L<sup>-1</sup>, or approximately 80% of the NO<sub>2</sub><sup>-</sup> inventory at that depth,  
565 enough that the NO<sub>2</sub><sup>-</sup> formation rate would no longer be correlated with chl *a* (e.g. because it is  
566 generated by non-photosynthetic microbes instead of phytoplankton). While the net NO<sub>2</sub><sup>-</sup>  
567 formation rate we calculated for 120 m contains some non-quantified input from NH<sub>4</sub><sup>+</sup>  
568 oxidation, the robust correlations between NO<sub>2</sub><sup>-</sup> formation and light and chl *a* at the other depths  
569 between 60-200m strongly suggest that NO<sub>3</sub><sup>-</sup> reduction was the dominant NO<sub>2</sub><sup>-</sup> forming process  
570 at these depths. However, the net NO<sub>2</sub><sup>-</sup> formation rates we report are not necessarily equivalent  
571 to NO<sub>3</sub><sup>-</sup> reduction rates by phytoplankton; they likely underestimate real NO<sub>3</sub><sup>-</sup> reduction rates  
572 because they do not account for processes that remove NO<sub>2</sub><sup>-</sup>, such as NO<sub>2</sub><sup>-</sup> oxidation during  
573 nitrification.

574

#### 575 **4. Discussion**

576 The Gulf of Aqaba has predictable seasonal patterns of NO<sub>2</sub><sup>-</sup> distribution, and the spring  
577 bloom is a period in which water column N dynamics transition between two different steady  
578 states. The changing physical, chemical, and biological characteristics of the water column  
579 during the onset of stratification in 2008 gave rise to substantial changes in the N cycle such that  
580 new steady state nutrient inventories were established. As the water chemistry shifted toward this  
581 new steady state different processes became dominant, giving rise to a PNM over a period of  
582 several days. Below we discuss these changes in the N cycle and how they lead to formation of  
583 the PNM which is maintained throughout the summer stratified period.

584

##### 585 **4.1 NO<sub>2</sub><sup>-</sup> dynamics during the transition from mixing to stratification**

586 The persistence of NO<sub>2</sub><sup>-</sup> in the ocean results from an imbalance in the processes that  
587 produce and consume NO<sub>2</sub><sup>-</sup> (**Fig.1**). In the aerobic water column, NO<sub>2</sub><sup>-</sup> is produced by NH<sub>4</sub><sup>+</sup>  
588 oxidizing organisms during the first step of nitrification, and by phytoplankton during  
589 incomplete NO<sub>3</sub><sup>-</sup> assimilation. It is consumed by NO<sub>2</sub><sup>-</sup> oxidizers during the second step of  
590 nitrification, and by phytoplankton during assimilation. Nitrite accumulates when production  
591 exceeds consumption as long as dispersion rates are sufficiently low. In the Gulf of Aqaba in  
592 winter, NO<sub>2</sub><sup>-</sup> is present at measurable concentrations throughout the mixed layer, whereas in the  
593 summer NO<sub>2</sub><sup>-</sup> accumulates below the euphotic zone, forming a PNM (**Fig. 2**; Al-Qutob et al.  
594 2002; Meeder et al. submitted).

595 To determine the role of phytoplankton in NO<sub>2</sub><sup>-</sup> formation, we considered the following  
596 three observations. First, *in winter* NO<sub>2</sub><sup>-</sup> was observed throughout the mixed layer, which is the

597 *depth of the water column occupied by phytoplankton, regardless of the exact mixing depth (Fig*  
598 *I). NO<sub>2</sub><sup>-</sup> did not accumulate below the mixing depth where phytoplankton do not survive. The*  
599 *mixed layer is the portion of the water column homogenized by turbulent mixing; for example,*  
600 *the mixed layer extended to the sea floor (~700m) in February 2008 (Fig. 2A), and to ~250 m in*  
601 *February 2003 (Fig. 2B). Phytoplankton can inhabit the whole mixed layer because water*  
602 *periodically gets mixed to the sunlit surface waters and allows for photosynthesis to occur*  
603 *(Smayda and Mitchell-Innes 1974); they cannot grow in the permanent darkness of the deep*  
604 *water below the mixing depth. NH<sub>4</sub><sup>+</sup> oxidizers, on the other hand, can occupy and grow*  
605 *throughout the entire water column including deep waters below the mixing depth because they*  
606 *do not require sunlight to survive. Therefore, if the major source of the NO<sub>2</sub><sup>-</sup> in winter were*  
607 *NH<sub>4</sub><sup>+</sup> oxidizers, then the accumulation of NO<sub>2</sub><sup>-</sup> would not be confined exclusively to the mixed*  
608 *layer, as we observe (Fig. 2). Second, the inverse relationship between NO<sub>3</sub><sup>-</sup> and NO<sub>2</sub><sup>-</sup> in winter*  
609 *profiles is maintained regardless of shoaling or deepening of the mixed layer during winter (Fig.*  
610 *2). This correlation suggests that NO<sub>3</sub><sup>-</sup> is the source of NO<sub>2</sub><sup>-</sup> generated within the mixed layer*  
611 *because as NO<sub>3</sub><sup>-</sup> is consumed NO<sub>2</sub><sup>-</sup> is produced. Third, the NO<sub>2</sub><sup>-</sup> and NO<sub>3</sub><sup>-</sup> inventories in the*  
612 *winter mixed layer agree well with the ratios of NO<sub>2</sub><sup>-</sup> to NO<sub>3</sub><sup>-</sup> observed during excretion by light*  
613 *limited phytoplankton following NO<sub>3</sub><sup>-</sup> uptake. Specifically, the fraction of NO<sub>2</sub><sup>-</sup> generated relative*  
614 *to NO<sub>3</sub><sup>-</sup> consumed in the mixed layer ranged from ~10% in 2003 (where ~0.4 μmol NO<sub>2</sub><sup>-</sup> L<sup>-1</sup> was*  
615 *generated and 4-6 μmol NO<sub>3</sub><sup>-</sup> L<sup>-1</sup> was consumed; Fig 2A) to ~15% in 2008 (where ~0.3 μmol*  
616 *NO<sub>2</sub><sup>-</sup> L<sup>-1</sup> was generated and 2 μmol NO<sub>3</sub><sup>-</sup> L<sup>-1</sup> was consumed; Fig. 3A). These ratios are*  
617 *consistent with the range of ratios measured in cultures of light limited phytoplankton that expel*  
618 *a portion of the NO<sub>3</sub><sup>-</sup> they take up as NO<sub>2</sub><sup>-</sup> (Collos 1998 and references therein). The non-*  
619 *nutritional uptake of NO<sub>3</sub><sup>-</sup> and release of NO<sub>2</sub><sup>-</sup> may be a mechanism by which certain*  
620 *phytoplankton regulate photosynthetic electron flow during periods when irradiance fluctuates*  
621 *(Lomas and Gilbert 1999, 2000), e.g. during deep mixing. Based on the above observations,*  
622 *phytoplankton appear to be the major source of NO<sub>2</sub><sup>-</sup> during convective winter mixing. These*  
623 *findings agree with an incubation study by Al-Qutob and co-workers (2002), in which NO<sub>2</sub><sup>-</sup> was*  
624 *produced by phytoplankton following N additions, and with monitoring studies conducted in this*  
625 *region (Meeder et al. in press).*

626 In a mixed water column, biological N transformation rates reflect the “average” light  
627 conditions because their products get distributed over the entire mixed layer. During winter in  
628 the Gulf of Aqaba, the mixing time (e.g. the time required for a parcel of water to complete one  
629 cycle of mixing from surface to the mixing depth and back to surface) is approximately 14 hr, 22  
630 hr, and 29 hr for mixing depths of 200 m, 400 m, and 600 m respectively based on typical heat  
631 flux and wind stress values for the region (S. Monismith, personal communication). The  
632 homogeneity of NO<sub>2</sub><sup>-</sup> in the mixed layer suggests that the mixing time is fast relative to the rates  
633 of NO<sub>2</sub><sup>-</sup> production and consumption such that no localized accumulation or drawdown of NO<sub>2</sub><sup>-</sup>  
634 is observed in the mixed layer.

635 In contrast, in a stratified water column organisms at any given depth are subject to  
636 relatively predictable light regimes. This allows different groups of organisms to populate depths  
637 they are best adapted to occupy. The PNM forms when stratification imposes a range of physical  
638 and chemical gradients on organisms, allowing different steady states to be reached between  
639 NO<sub>2</sub><sup>-</sup> production and consumption at different depths in the water column. This is evident from  
640 summer profiles of NO<sub>2</sub><sup>-</sup> from 2003 and 2008, where NO<sub>2</sub><sup>-</sup> accumulates at ~100 m, but not in  
641 surface or deep waters. These monthly “snapshots” provide information on steady state nutrient  
642 levels; they integrate and reflect the net result of all processes that produce and consume NO<sub>2</sub><sup>-</sup> at



643 a given depth.

644 The individual contributions of specific N transformation processes on PNM formation  
645 can be discerned from the higher frequency monitoring data collected during the spring bloom.  
646 To focus our discussion, we define four principal regions of the water column based on light  
647 attenuation and major features of the PNM (**Fig. 9**). The “euphotic zone” (0-60 m during our  
648 study), extends from the surface to the compensation depth (i.e., the depth at which light is  
649 attenuated to 1% of surface irradiance). The “sub-euphotic zone” (60-160 m during our study),  
650 extends to the top of the PNM. The “upper PNM” (180-225 m during our study), encompasses  
651 depths with substantial accumulation of  $\text{NO}_2^-$ . The “disphotic zone” extends from the depth  
652 where the  $\text{NO}_2^-$  concentrations of the PNM starts decreasing down to the sea floor (below 225 m  
653 during our study). We note that the absolute depths given above for our study are not universal  
654 for all summers in the Gulf of Aqaba or for all water columns because they would change  
655 depending on the depth of the mixed layer prior to stratification, latitude, amount of chl *a*  
656 present, and other factors influencing light penetration. Below we describe how N cycling  
657 processes that produce and consume  $\text{NO}_2^-$  generate conditions that give rise to the PNM.

658

#### 659 **4.1.1 Euphotic zone.**

660 The euphotic zone is the layer in which sufficient light is available for photosynthesis to  
661 exceed respiration, and where the majority of photosynthetic biomass is generated. Uptake of  
662  $\text{NO}_3^-$  and  $\text{NH}_4^+$  is at times light dependent in natural phytoplankton populations, with the highest  
663 rates generally occurring in the surface ocean and decreasing with depth as light becomes  
664 attenuated (MacIsaac and Dugdale 1972). This trend was observed in the euphotic zone of the  
665 Gulf as stratification became established. DIN uptake by phytoplankton was highest in surface  
666 waters and lower at the base of the euphotic zone (**Fig. 3A**).

667 Most of the available  $\text{NO}_3^-$  and  $\text{NO}_2^-$  in the euphotic zone of the Gulf of Aqaba was  
668 assimilated and converted into biomass (e.g. photosynthetic uptake) (**Fig. 3**) between March 18  
669 and 25. However, results suggest that mineralization and subsequent nitrification of organic N  
670 played an important role in the euphotic zone, where DIN concentrations were low due to  
671 efficient phytoplankton uptake. Between March 18 and March 25  $\delta^{15}\text{N}_{\text{N+N}}$  increased by 8 ‰ in  
672 comparison to 45 ‰ for  $\delta^{18}\text{O}_{\text{N+N}}$  (most enriched values seen on March 24) in surface samples  
673 (e.g., upper 20m), causing high  $\delta^{18}\text{O}_{\text{N+N}} : \delta^{15}\text{N}_{\text{N+N}}$  ratios relative to the rest of the water column  
674 on March 24 and 25. The increasing slope of  $\delta^{18}\text{O}_{\text{N+N}} : \delta^{15}\text{N}_{\text{N+N}}$  (up to 5) indicates decoupling of  
675 the N and O isotopes of nitrate, which suggests an important role for assimilation and recycling,  
676 e.g. nitrification, in the euphotic zone. The decoupling is a result of the branching during  $\text{NH}_4^+$   
677 consumption in which  $\text{NH}_4^+$  serves as a substrate for regenerated production and for nitrification.  
678 The difference between the isotope effects of these two processes controls the  $\delta^{15}\text{N}$  of the  $\text{NO}_3^-$   
679 returned to the N pool, whereas the O is insensitive to the origin of the N (Wankel et al, 2007).  
680 This greater enrichment of O relative to N due to co-occurring assimilation and nitrification has  
681 also been observed in surface waters in Monterey Bay (Wankel et al. 2007), where regenerated N  
682 supports 15-27% of  $\text{NO}_3^-$  based production.

683  $\delta^{15}\text{N}_{\text{N+N}}$  and  $\delta^{18}\text{O}_{\text{N+N}}$  can be affected by factors other than assimilation and nitrification,  
684 such as those that contribute  $\text{NO}_3^-$  with different isotopic compositions than deep water N+N.  
685 For example, atmospheric dry deposition has been shown to be a substantial contributor of  
686 relatively light N and heavy O to the Gulf of Aqaba (summer average  $\delta^{15}\text{N}$  -1.7 ‰ and  $\delta^{18}\text{O}$   
687 77.3‰; Wankel et al. 2009). Another potential source of light N in surface water (**Fig. 5A**) is  
688 biological  $\text{N}_2$  fixation, which reflects the  $\delta^{15}\text{N}$  of atmospheric  $\text{N}_2$  gas that is by definition zero.

689 Measurements of N<sub>2</sub> fixation rates in the Gulf have ranged from below detection (Hadas and Erez  
690 2004) to low but measurable rates of 1-2 nmol L<sup>-1</sup> day<sup>-1</sup> (Foster et al. 2009). These rates are small  
691 compared to other N transformation rates measured for the Gulf (**Table 1**). However, we did not  
692 measure N<sub>2</sub> fixation or atmospheric deposition directly in this study, so a contribution from  
693 either cannot be confirmed or ruled out. Preferential export of <sup>15</sup>N in particulate matter out of the  
694 euphotic zone (Altabet 1988) can skew the δ<sup>18</sup>O<sub>N+N</sub> : δ<sup>15</sup>N<sub>N+N</sub> relationship in surface waters, and  
695 is apparent from the increased δ<sup>15</sup>N of particulate N with depth as the bloom progressed (**Fig.**  
696 **5C**), although fractionation during mineralization could also contribute to this signal.

#### 697 698 **4.1.2 Sub-euphotic zone.**

699 In this zone light is attenuated below the compensation threshold, and respiration by the  
700 entire microbial community is likely to exceed photosynthesis by phytoplankton. Regression  
701 analysis for depths in the sub-euphotic zone and down to 200 m showed that net NO<sub>2</sub><sup>-</sup> production  
702 rates correlated very strongly with decreasing irradiance (**Fig. 8B**). However, regression analysis  
703 of residual chl *a* and residual NO<sub>2</sub><sup>-</sup> production data (i.e. with the influence of irradiance  
704 removed) also showed a remarkably strong correlation (**Fig. 8D**), and suggested that NO<sub>3</sub><sup>-</sup> uptake  
705 and released as NO<sub>2</sub><sup>-</sup> by light limited phytoplankton was the dominant N transformation process  
706 in the sub-euphotic zone during the beginning of the bloom (March 18-24). These results agree  
707 with the findings of Dore & Karl (1996a) in the Pacific Ocean, where they suggest that the upper  
708 portion of the PNM is generated by phytoplankton NO<sub>2</sub><sup>-</sup> release and closely tracks the nitricline.

709 An exception occurred at 120 m, where a large portion of NO<sub>2</sub><sup>-</sup> was generated from NH<sub>4</sub><sup>+</sup>  
710 oxidation rather than NO<sub>3</sub><sup>-</sup> reduction based on regression statistics (**Fig. 3A; Fig. 8D**). The  
711 contribution of NH<sub>4</sub><sup>+</sup> oxidation to the NO<sub>2</sub><sup>-</sup> formation over this range of depths suggests that  
712 substrate limitation of NH<sub>4</sub><sup>+</sup> oxidation rates may be impacting NO<sub>2</sub><sup>-</sup> distribution in the water  
713 column (Ward 1985). Our data shows that NO<sub>2</sub><sup>-</sup> formation from NH<sub>4</sub><sup>+</sup> oxidation can match or  
714 exceed NO<sub>3</sub><sup>-</sup> reduction where ample NH<sub>4</sub><sup>+</sup> is available. Indeed, the increasing slope of the best fit  
715 line for δ<sup>18</sup>O<sub>N+N</sub> : δ<sup>15</sup>N<sub>N+N</sub> over this range of depths (Fig. 6, orange circles) indicates that  
716 nitrification was occurring within the sub-euphotic zone.

717 While the sub-euphotic zone is below the compensation depth, it is important to note that  
718 phytoplankton continue to take up nutrients and perform photosynthesis in this dim layer (these  
719 rates are simply exceeded by respiration rates). The δ<sup>15</sup>N<sub>N+N</sub> was elevated in the sub-euphotic  
720 zone with respect to deeper water as the bloom progressed (**Fig. 5A**), indicating that assimilation  
721 of N+N by phytoplankton or other microbes takes place. While seemingly counterintuitive that  
722 phytoplankton could be both a source and a sink for NO<sub>2</sub><sup>-</sup> in the sub-euphotic zone over the  
723 course of a bloom, several processes could lead to this outcome. First, intermittent changes in  
724 light intensity due to internal waves could lead phytoplankton at the base of the sub-euphotic  
725 zone to toggle between NO<sub>3</sub><sup>-</sup> assimilation and NO<sub>2</sub><sup>-</sup> excretion depending on their light  
726 requirements. Another factor is that the phytoplankton community is a diverse assemblage of  
727 different sub-populations, each with its own light requirements and N assimilation strategies.  
728 During the bloom succession occurs within the phytoplankton community, and different sub-  
729 populations coexist, compete, and eventually either survive or get out-competed. Therefore,  
730 while one sub-population may take up NO<sub>3</sub><sup>-</sup> and release NO<sub>2</sub><sup>-</sup> due to light limitation, another may  
731 be able to complete the assimilation of NO<sub>3</sub><sup>-</sup> into biomass. Between March 24-25  
732 nanophytoplankton abundance increased in the sub-euphotic zone (**Fig. 4**). Nanophytoplankton  
733 include phytoplankton taxa such as diatoms, and monitoring conducted after our sampling period  
734 showed that the spring bloom became dominated by diatoms by the beginning of April (Iluz et

735 al. 2009). Non-nutritional uptake of  $\text{NO}_3^-$  has been observed in some marine diatoms (Lomas and  
736 Gilbert 1999), and uptake (though not necessarily assimilation) by these comparatively large  
737 cells may have played a role in the drawdown of  $\text{NO}_3^-$  and  $\text{NO}_2^-$  in the sub-euphotic zone. Light-  
738 independent assimilation of  $\text{NO}_3^-$  and  $\text{NO}_2^-$  by non-photosynthetic microbes, which were  
739 abundant throughout the water column, could also have caused the high  $\delta^{15}\text{N}_{\text{N+N}}$  values at these  
740 dim depths (Tupas et al. 1994).

741

#### 742 **4.1.3 The upper PNM.**

743 The upper PNM (180-225 m) is a dynamic region where  $\text{NO}_2^-$  accumulates. Within this  
744 layer light is attenuated to levels too low for photosynthesis (**Fig. 8A**). During the first part of the  
745 bloom  $\text{NO}_2^-$  dynamics in the upper PNM were similar to the sub-euphotic zone in that  $\text{NO}_2^-$   
746 production was strongly correlated with chl *a* levels, implicating phytoplankton as the main  
747 source of  $\text{NO}_2^-$  (**Fig. 8**). However, over the next day, net  $\text{NO}_2^-$  production continued within the  
748 upper region of the PNM and was no longer correlated to chl *a* (data not shown). The  $\text{NO}_2^-$   
749 produced by phytoplankton during the first part of the bloom was derived from  $\text{NO}_3^-$  taken up  
750 during the mixed period (e.g. March 18) when, due to mixing, light was episodically high  
751 enough to support  $\text{NO}_3^-$  uptake. Following stratification phytoplankton trapped below the  
752 euphotic depth would have expelled that N as  $\text{NO}_2^-$  due to a lack of light energy needed to  
753 complete the assimilation process. However, by March 24 phytoplankton trapped within the  
754 upper PNM would have been without sufficient light for approximately one week. It is unlikely  
755 that these cells could initiate de novo uptake of fresh  $\text{NO}_3^-$  and be the source of  $\text{NO}_2^-$  generated at  
756 this depth between March 24 and 25.  $\text{NH}_4^+$  oxidizers, on the other hand, would have access to an  
757 increasingly large pool of DON from which to access their  $\text{NH}_4^+$  substrate following  
758 ammonification.

759  $\text{NO}_2^-$  can only accumulate if production exceeds consumption and dispersion is  
760 sufficiently low. The  $\text{NO}_2^-$  accumulation in the upper PNM (180-225 m) during the second part  
761 of the bloom indicates that  $\text{NO}_2^-$  production and consumption were decoupled, with production  
762 exceeding consumption. Nitrification was the major source of  $\text{NO}_2^-$  in the upper PNM once  
763 phytoplankton  $\text{NO}_2^-$  excretion had declined following the initial stages of stratification. The main  
764  $\text{NO}_2^-$  consuming process at these depths was  $\text{NO}_2^-$  oxidation because photosynthetic  $\text{NO}_2^-$   
765 assimilation is light limited at these dark depths. The steep slope of  $\delta^{18}\text{O}_{\text{N+N}}$ :  $\delta^{15}\text{N}_{\text{N+N}}$  values for  
766 N+N shows that nitrification was occurring over this range of depths by March 25 when  
767 stratification was firmly established (Fig. 6, green circles). Olsen (1981) postulated that the  
768 greater sensitivity of  $\text{NO}_2^-$  oxidizers than  $\text{NH}_4^+$  oxidizers to light could be a mechanism by which  
769 PNM form. Guerrero and Jones (1996) added to this model, noting that  $\text{NH}_4^+$  oxidizers recover  
770 more rapidly from photoinhibition than do  $\text{NO}_2^-$  oxidizers. Based on these observations,  $\text{NH}_4^+$   
771 oxidizers are postulated to be more active in shallower regions of the water column than  $\text{NO}_2^-$   
772 oxidizers, and this spatial segregation of the populations leads to accumulation of  $\text{NO}_2^-$ .

773 The pattern of PNM formation in the Gulf of Aqaba is consistent with these hypotheses  
774 of differential photoinhibition and recovery based on the concentrations of  $\text{NH}_4^+$ ,  $\text{NO}_2^-$ , and  $\text{NO}_3^-$   
775 throughout the water column. The  $\text{NO}_3^-$  concentration data suggests that  $\text{NO}_2^-$  oxidation was  
776 closely coupled to  $\text{NH}_4^+$  oxidation *only* at depths below ~225 m, where production of  $\text{NO}_3^-$  was  
777 observed concurrently with  $\text{NH}_4^+$  and  $\text{NO}_2^-$  consumption (**Fig. 3A**). At these dark depths no  $\text{NO}_2^-$   
778 accumulated, consistent with a lack of photoinhibition of either  $\text{NH}_4^+$  or  $\text{NO}_2^-$  oxidizers. In  
779 contrast, above the upper PNM (140-180 m)  $\text{NH}_4^+$  accumulated and resulted in an  $\text{NH}_4^+$  peak by  
780 March 25. The light levels at these depths may have been sufficiently high to inhibit  $\text{NH}_4^+$

781 oxidation rates in keeping with the hypotheses discussed above, thereby allowing  $\text{NH}_4^+$  to  
782 accumulate. However, within the upper PNM depths of 180-225m,  $\text{NO}_3^-$  and  $\text{NO}_2^-$  accumulated  
783 concurrently, suggesting that  $\text{NH}_4^+$  oxidation was continuing while  $\text{NO}_2^-$  oxidation was slowing,  
784 an observation that could be explained by differential photosensitivity of the two nitrifier  
785 populations. However, recovery from photoinhibition must have been reversible over the diel  
786 cycle, as the isotope data strongly indicate a complete nitrification cycle within the euphotic zone  
787 and upper PNM in the Gulf of Aqaba.  
788

#### 789 **4.1.4 The Disphotic Zone.**

790 The disphotic zone contains the lower portion of the PNM (225-300 m; **Fig. 3A**) as well  
791 as deep water. Within the disphotic zone, sunlight is attenuated to less than 0.001% of surface  
792 irradiance and phytoplankton are unable to perform photosynthesis. Therefore, non-  
793 photosynthetic microbial processes dominate the N cycle at these depths, and indeed, several  
794 observations are indicative of a nitrification-dominated system. As noted above,  $\text{NH}_4^+$  and  $\text{NO}_2^-$   
795 were consumed while net  $\text{NO}_3^-$  production occurred below 225 m, consistent with microbially  
796 mediated oxidation of  $\text{NH}_4^+$  and  $\text{NO}_2^-$  into  $\text{NO}_3^-$ . Microbial nitrification in the disphotic zone  
797 also refined the shape of the lower PNM during the onset of stratification by consuming a portion  
798 of the broad band of  $\text{NO}_2^-$  that was generated during the beginning of stratification, and helped  
799 maintain the characteristic shape of the PNM throughout the summer. This can be seen on March  
800 25, where the falling limb of the PNM took on a steeper slope than on March 24 (**Fig. 3A**) and  
801 was more similar to summer profiles from other years (**Fig. 2**).

802 The elevated  $\delta^{15}\text{N}$  of particulate N that was spread throughout the water column by  
803 March 25 (**Fig. 5C**) also suggests that a link exists between phytoplankton growth in the surface  
804 and mineralization/nitrification at depth. Active processes, such as selective zooplankton grazing  
805 and excretion, play an important role in packaging smaller suspended particles, such as  
806 phytoplankton cells, within the euphotic zone for export as sinking particles. As a result, sinking  
807 particles are generally higher in  $\delta^{15}\text{N}$  than suspended particles within the euphotic zone (Altabet  
808 1988). The transport of sinking particles occurred quickly, as the elevated  $\delta^{15}\text{N}_{\text{part}}$  was already  
809 spread throughout the water column within days of the bloom initiating (**Fig. 5C**). The sinking of  
810 particulate matter from the surface to deep water is likely to be an important source of N that  
811 fuels nitrification in the disphotic zone throughout the stratified period, and recharges the  $\text{NO}_3^-$   
812 reservoir at depth.

813 Values for  $\delta^{15}\text{N}_{\text{N+N}}$  and  $\delta^{18}\text{O}_{\text{N+N}}$  in the disphotic zone varied little over the time period  
814 studied ( $\delta^{15}\text{N}_{\text{N+N}}$  was  $\sim 2.5$  and  $\delta^{18}\text{O}_{\text{N+N}}$  was  $\sim 6.5$ ), but were distinct from those observed for  
815 open ocean deep water nitrate; ( $\delta^{15}\text{N}$  5 ‰ (Sigman et al. 2000) and  $\delta^{18}\text{O}$  2 ‰ (Knapp et al.  
816 2008). Low  $\delta^{15}\text{N}$  with respect to deep water  $\text{NO}_3^-$  has also been observed in the Mediterranean  
817 Sea (Pantojo et al, 2002). Potential causes include  $^{15}\text{N}$  depleted sources such as  $\text{N}_2$  fixation and  
818 atmospheric deposition along with the lack of water column denitrification and its associated  
819 large isotope effect ( $\sim 25$  ‰, Cline and Kaplan, 1975) and the restricted exchange of these  
820 systems with the open ocean. The higher  $\delta^{18}\text{O}_{\text{N+N}}$  values may be partially due to the higher  $\delta^{18}\text{O}$   
821 of water in the Gulf of Aqaba corresponding to its elevated salinity, and on a regional scale the  
822 higher  $\delta^{18}\text{O}$  signal in water would be transferred to  $\text{NO}_3^-$  via nitrification (Casciotti et al, 2010).  
823 Atmospheric deposition in this region is another source of  $\text{NO}_3^-$  with higher  $\delta^{18}\text{O}_{\text{N+N}}$  (Wankel et  
824 al. 2009).  
825

## 826 **4.2 N uptake and regeneration in the Gulf of Aqaba**

827 Our measurements for uptake of  $\text{NO}_3^-$  (26-434  $\text{nmol N L}^{-1} \text{ day}^{-1}$ ) and  $\text{NH}_4^+$  (314  $\text{nmol N}$   
828  $\text{L}^{-1} \text{ day}^{-1}$ ) are in good agreement with uptake estimates from other studies for  $\text{NO}_3^-$  (ranging from  
829 48-526  $\text{nmol N L}^{-1} \text{ day}^{-1}$ ) and  $\text{NH}_4^+$  (40-1536  $\text{nmol N L}^{-1} \text{ day}^{-1}$ ) in a range of environments and  
830 for different light intensities (Bronk et al. 1994; Wheeler and Kirchman 1986; Probyn and  
831 Painting 1985; McCarthy 1972). Fewer measurements of  $\text{NO}_2^-$  uptake are available; however, an  
832 approximation can be made based on the cell specific  $\text{NO}_2^-$  uptake rate determined for  
833 *Synechococcus* 7803 (0.02  $\text{fmol cell}^{-1} \text{ hr}^{-1}$ ; Lindell et al. 1998). This would correspond to a  $\text{NO}_2^-$   
834 uptake rate of  $\sim 80 \text{ nmol N L}^{-1} \text{ day}^{-1}$  based on the phytoplankton cell abundances measured  
835 during our study ( $\sim 1.70 \times 10^5 \text{ c mL}^{-1}$ ), and is consistent with the range of uptake rates we measured  
836 in our  $^{15}\text{N}$  tracer experiment (29-94  $\text{nmol N L}^{-1} \text{ day}^{-1}$ ). Urea uptake rates encompass a much  
837 broader set of values in the environment, ranging from  $<2.4$  to 86,400  $\text{nmol N L}^{-1} \text{ hr}^{-1}$   
838 (Kristiansen 1983, Berg et al. 1997, Lomas et al. 2002, Berman & Bronk 2003), and our  
839 measured rates of 296-1285  $\text{nmol N L}^{-1} \text{ hr}^{-1}$  fall within that range. We note that spontaneous  
840 decomposition of urea into  $\text{NH}_4^+$  can occur in the light and were determined to be  $\sim 240 \text{ nmol L}^{-1}$   
841  $\text{day}^{-1}$  in the Gulf of Aqaba (Kamennaya et al. 2008). However, this rate was measured following  
842 a relatively concentrated urea spike of 20  $\mu\text{mol N L}^{-1}$ , compared to our dilute spike of 0.2  $\mu\text{mol}$   
843  $\text{N L}^{-1}$ . If degradation kinetics are similar over this range of urea concentrations, then spontaneous  
844 degradation of urea to  $\text{NH}_4^+$  could have caused an overestimation of  $\sim 20\%$  for our urea uptake  
845 rates in the light.

846 The N cycle in the Gulf of Aqaba provides an example of a system with closely coupled  
847 N assimilation and regeneration during the stratified period. The increasing slope of the best fit  
848 line for  $\delta^{18}\text{O}_{\text{N+N}}: \delta^{15}\text{N}_{\text{N+N}}$  (from 2:1-5:1; **Fig. 6**) indicates that regenerated organic matter is a  
849 major source of N for primary producers in the Gulf of Aqaba, because it shows a strong  
850 signature of uncoupled fractionation of N and O that is imparted during nitrification. This  
851 observation is consistent with other studies that have found high rates of primary productivity  
852 despite relatively low standing stocks of phytoplankton in the Gulf (Hase et al. 2006). Together  
853 these findings suggest that assimilation and nitrification compete for  $\text{NH}_4^+$ , and that primary  
854 productivity is tightly coupled to grazing food webs and microbial remineralization processes,  
855 which are a source of  $\text{NH}_4^+$ . Productivity is therefore partially supported by efficient  
856 sequestration of  $\text{NH}_4^+$  within cells as soon as it becomes available, in addition to using  $\text{NO}_3^-$   
857 produced during nitrification.

858 During our monitoring of the spring bloom the concentration of DON increased by 1.1  
859  $\mu\text{mol N L}^{-1}$  as DIN decreased by this amount (**Fig. 3B**). Labile DON could play an important  
860 role in the Gulf's biogeochemical cycling of N and serve as an important nutrient resource for  
861 non-photosynthetic microbes and marine phytoplankton, similar to other areas of the ocean  
862 (Solomon et al. 2010; Palenik and Morel 1990; Moore et al. 2002; Zubkov et al. 2003). The role  
863 of labile DON could be particularly important in ultra-oligotrophic marine environments where  
864 DIN concentrations are very low and the reservoir of DON can be over an order of magnitude  
865 larger than DIN, as was the case in the Gulf of Aqaba where DON reached  $\sim 10 \mu\text{mol N L}^{-1}$  and  
866 the  $\text{NO}_3^-$  concentration was 0.1-0.2  $\mu\text{mol L}^{-1}$  (March 25). Moreover, in some marine diatoms  
867  $\text{NH}_4^+$  and DON uptake rates increase with temperature while  $\text{NO}_3^-$  uptake rates decrease (Lomas  
868 and Gilbert 1999), suggesting that DON could be the preferred source of N for phytoplankton  
869 that bloom in warming surface waters as stratification becomes established.

870 In the Gulf of Aqaba where ammonification and nitrification are closely coupled,  $\text{NH}_4^+$   
871 generated during mineralization of DON should be considered when making measurements of  
872  $\text{NH}_4^+$  oxidation. Calculations based on  $^{15}\text{N}$  labeling data are complicated by rapid and closely

873 coupled  $\text{NH}_4^+$  production and consumption, and can result in rate underestimation. In this study  
874 the rate of coupled mineralization and  $\text{NH}_4^+$  oxidation were measured in the  $^{15}\text{N}$  tracer  
875 experiment for urea, a labile form of DON. The overall rate of coupled urea mineralization and  
876  $\text{NH}_4^+$  oxidation ( $14.1 \text{ nmol N L}^{-1} \text{ day}^{-1}$ ) was remarkably similar to that of  $\text{NH}_4^+$  oxidation alone  
877 based on our study ( $16.4 \text{ nmol N L}^{-1} \text{ day}^{-1}$ ) and other studies ( $\sim 18\text{-}40 \text{ nmol N L}^{-1} \text{ day}^{-1}$ ; Ward  
878 2005; Ward et al. 1982), suggesting that mineralization is not a rate limiting step for nitrification,  
879 at least when the DON pool is relatively large and labile. The composition and lability of DON  
880 changes based on community composition, grazing rates, mixing, and numerous other factors,  
881 although estimates suggest that complete DON turnover occurs on the order of 10 days in  
882 oligotrophic waters (Bronk et al. 1994). Rates measured for labile DON compounds, such as urea  
883 in this study, provide maximum potential rates for DON mineralization and nitrification. Actual  
884 rates will be lower, and mineralization may limit nitrification rates for  $\text{NH}_4^+$  derived from more  
885 refractory forms of DON. More work is needed to characterize the DON pools in different waters  
886 and determine their influence on marine nitrification rates.

## 887 5. Conclusion

888 This study used isotope data from natural abundance samples in the Gulf of Aqaba  
889 together with tracer experiments to identify important processes in the N cycle and quantify their  
890 rates. The approach has highlighted the importance of regenerated N for supporting productivity  
891 in the Gulf of Aqaba, where efficient photosynthetic sequestration of N in surface waters is  
892 coupled to mineralization and nitrification of PON and DON throughout the water column.  
893 Export and regeneration (mineralization and nitrification) of particulate N to DIN at depth serves  
894 to recharge the  $\text{NO}_3^-$  reservoir in deep water.

895 Several major light-sensitive processes contribute to the formation of PNM in the Gulf of  
896 Aqaba during the transition from mixing to stratification. Within the euphotic zone,  
897 phytoplankton assimilate N during growth by drawing down DIN levels sharply in the well-lit  
898 surface waters. Below the euphotic depth during the initial stages of stratification, a large  
899 inventory of  $\text{NO}_2^-$  is generated from incomplete  $\text{NO}_3^-$  reduction by trapped, light limited  
900 phytoplankton.  $\text{NO}_2^-$  from this process is distributed over a range of depths, creating a broad  
901 band of  $\text{NO}_2^-$  with a subsurface peak. Later, once stratification is firmly established, net  $\text{NO}_2^-$  is  
902 generated by  $\text{NH}_4^+$  oxidizers over a narrower range of depths coinciding with the upper part of  
903 the PNM, and is consistent with differential light inhibition of  $\text{NH}_4^+$  and  $\text{NO}_2^-$  oxidizing  
904 communities. Deeper in the water column where light is negligible,  $\text{NO}_2^-$  oxidation rates match  
905  $\text{NH}_4^+$  oxidation, and  $\text{NO}_2^-$  gets drawn down, defining the lower portion of the PNM.

906 Mineralization and subsequent nitrification of organic material is an important source of  
907 N for primary producers in the Gulf of Aqaba, where  $\text{NO}_3^-$  formed from nitrification of  $\text{NH}_4^+$  and  
908 urea (following ammonification) at rates of similar magnitude. The similar magnitudes of  
909 assimilation rates for urea and  $\text{NO}_3^-$  suggest that labile organic N is an important source of N for  
910 primary producers in this oligotrophic region during the stratified season. The rate and type of N  
911 transformation processes operating throughout the water column are strongly influenced by light,  
912 which determines the maximum depths for net photosynthesis and may contribute to inhibition  
913 of nitrifying communities.

914  
915

916 **Table 1:** N transformation rates determined in the  $^{15}\text{N}$  tracer experiment. N assimilation rates  
 917 into particulate biomass for  $\text{NO}_3^-$ ,  $\text{NO}_2^-$ , urea, and  $\text{NH}_4^+$ , as well as  $\text{NO}_2^-$  formation rates from  
 918  $\text{NH}_4^+$  and urea are shown. “N addition” indicates the form of  $^{15}\text{N}$  enriched spike added. “Light”  
 919 uptake rates indicate bottles incubated at 50% surface sunlight irradiance, and “dark” uptake  
 920 rates indicate bottles incubated in full darkness.

N addition	Process	Experiment number	Time (hr)	Light rate (nmol N L <sup>-1</sup> day <sup>-1</sup> )*	Dark rate (nmol N L <sup>-1</sup> day <sup>-1</sup> )*
$\text{NO}_3^-$	assimilation	1	1	ND	26±0.00
$\text{NO}_3^-$	assimilation	1	7	434±24	58±14
$\text{NO}_3^-$	assimilation	1	13	415±103	65±19
$\text{NO}_3^-$	assimilation	2	1	ND	41±2.4
$\text{NO}_3^-$	assimilation	2	13	420±82	137±79
$\text{NO}_2^-$	assimilation	2	1	ND	29±12
$\text{NO}_2^-$	assimilation	2	7	94±17	29±14
$\text{NO}_2^-$	assimilation	2	13	ND	ND
Urea	assimilation	1	1	ND	296±40
Urea	assimilation	1	7	1194±48	476±31
Urea	assimilation	1	13	1285±32	308±10
Urea	reminerzalization and oxidation to $\text{NO}_2^-$	1	1	ND	14.1±7.6
$\text{NH}_4^+$	assimilation	2	1	ND	314±31
$\text{NH}_4^+$	assimilation	2	7	ND	ND
$\text{NH}_4^+$	assimilation	2	13	ND	ND
$\text{NH}_4^+$	oxidation to $\text{NO}_2^-$	2	1	ND	16.4±8.1

921 \*Values reported are the mean ± standard error of triplicate measurements from independent  
 922 bottles (i.e., three independent bottles per treatment per time point).  
 923 ND indicates that the rate was not determined. The second time interval of 13 hrs was not used  
 924 for some samples because all of the  $^{15}\text{N}$  spike had been exhausted (taken up) within the first 7 hrs  
 925 of incubation (see text). The rates in the light were not determined for 1hour time points because  
 926 they were measured before dawn.  
 927

928 **Table 2:** Net  $\text{NO}_2^-$  production rates.  $\text{NO}_2^-$  production was dominated by  $\text{NO}_3^-$  reduction by  
 929 phytoplankton at depths of 60, 80, 160, and 200 m, and by  $\text{NH}_4^+$  oxidation by nitrifying microbes  
 930 at 120 m ( $\text{NH}_4^+$  oxidation, see Fig. 8D and text for explanation). Rates were calculated from the  
 931 change in concentration of  $\text{NO}_2^-$  between March 18 and March 24 at the onset of stratification,  
 932 and are given on a per volume basis as well as on a per unit chl *a* basis. No values were  
 933 calculated for 180 m because this depth was not sampled on March 18, so no change in  $\text{NO}_2^-$   
 934 concentration could be calculated.  
 935

Depth (m)	Light attenuation (% surface PAR)	$\Delta [\text{NO}_2^-]$ ( $\text{nmol L}^{-1}$ )	chl <i>a</i> ( $\mu\text{g L}^{-1}$ )	$\text{NO}_2^-$ production rate ( $\text{nmol L}^{-1} \text{ day}^{-1}$ )	$\text{NO}_2^-$ production rate ( $\text{nmol } \mu\text{g chl } a^{-1} \text{ day}^{-1}$ )
60	1	13	0.44	2.2	5.0
80	0.2	58	0.39	9.7	25
120	0.01	143	0.26	24	NA
160	0.0004	275	0.17	46	270
200	0.00002	345	0.19	58	290

936  
 937 NA indicates “not applicable” because the source of  $\text{NO}_2^-$  was  $\text{NH}_4^+$  oxidizers rather than  
 938 phytoplankton at this depth, so the rate was not normalized to chl *a*.  
 939



940 **References**

- 941
- 942 Allen, A. E., M. G. Booth, M. E. Frischer, P. G. Verity, J. P. Zehr, and S. Zani (2001), Diversity  
943 and detection of nitrate assimilation genes in marine bacteria, *Applied and Environmental*  
944 *Microbiology* 67, 5343-5348.
- 945 Allen, A. E., M. G. Booth, P. G. Verity, M. E. Frischer (2005) Influence of nitrate availability on  
946 the distribution and abundance of heterotrophic bacterial nitrate assimilation genes in the  
947 Barents Sea during summer, *Aquatic Microbial Ecology* 39, 247–255.
- 948 Al-Qutob, M., C. Hase, M. M. Tilzer, B. Lazar (2002), Phytoplankton drives nitrite dynamics in  
949 the Gulf of Aqaba, Red Sea. *Marine Ecology Progress Series*. 239, 233-239.
- 950 Altabet, M. A. 1988. Variations in nitrogen isotopic composition between sinking and suspended  
951 particles: implications for nitrogen cycling and particle transformation in the open ocean.  
952 *Deep-Sea Research* 35, 535-554.
- 953 Bronk, D. A., P. M. Gilbert, and B. B. Ward (1994), Nitrogen uptake, dissolved organic nitrogen  
954 release, and new production. *Science* 265, 1843-1846.
- 955 Cai, H. and N. Jiao (2008), Diversity and Abundance of Nitrate Assimilation Genes in the  
956 Northern South China Sea. *Microb Ecol* 56, 751–764 DOI 10.1007/s00248-008-9394-7.
- 957 Casciotti, K. L. (2009), Inverse kinetic isotope fractionation during bacterial nitrite oxidation.  
958 *Geochimica et Cosmochimica Acta*. 73, 2061-2076.
- 959 Casciotti, K. L., M. McIlvin, C. Buchwald (2010), Oxygen isotopic exchange and fractionation  
960 during bacterial ammonia oxidation. *Limnology and Oceanography* 55, 753–762.
- 961 Casciotti, K. L., D. M. Sigman, M. Galanter-Hastings, J. K. Bohlke, and A. Hilkert (2002),  
962 Measurement of the Oxygen Isotopic Composition of Nitrate in Seawater and Freshwater  
963 Using the Denitrifier Method. *Analytical Chemistry*, 74, 4905–4912.
- 964 Casciotti, K. L. and B. B. Ward (2006), Phylogenetic analysis of nitric oxide reductase gene  
965 homologues from aerobic ammonia-oxidizing bacteria. *FEMS Microbiology Ecology* 52,  
966 197-205.
- 967 Casciotti, K. L., and B. B. Ward (2001), Dissimilatory Nitrite Reductase Genes from Autotrophic  
968 Ammonia-Oxidizing Bacteria *Applied and Environmental Microbiology*, 67, 2213-  
969 2221 DOI: 10.1128/AEM.67.5.2213-2221.2001.
- 970 Cohen Y. and M. Ottolenghi (2004), Gulf of Eilat Monitoring and Research Program -IET :  
971 Recommendations - Final Report.  
972 [http://sviva.gov.il/Environment/Static/Binaries/Articals/final\\_report04\\_1.pdf](http://sviva.gov.il/Environment/Static/Binaries/Articals/final_report04_1.pdf)
- 973 Collier, J. L., B. Brahamsha and B. Palenik (1999), The marine cyanobacterium *Synechococcus*  
974 sp. WH7805 requires urease (urea amiohydrolase, EC 3.5.1.5) to utilize urea as a nitrogen  
975 source: molecular-genetic and biochemical analysis of the enzyme. *Microbiology* 145,  
976 447-459; DOI 10.1099/13500872-145-2-447.
- 977 Collos, Y. (1998), Nitrate, nitrite release and uptake, and new production estimates. *Marine*  
978 *Ecology Progress Series* 171, 293-301.
- 979 Cornell, S., A. Randell, and T. Jickells (1995), Atmospheric inputs of dissolved organic nitrogen  
980 to the oceans. *Nature* 376, 243 – 246.
- 981 D'Elia, C.F., P.A. Steudler, and N. Corwin (1977) Determination of total nitrogen in aqueous  
982 samples using persulfate digestion. *Limnology and Oceanography* 22, 760-764.
- 983 DeNiro M. J. and S. Epstein (1981), Influence of diet on the distribution of nitrogen isotopes in  
984 animals. *Geochimica et Cosmochimica Acta* 45, 341-351.
- 985

986 Dore, JE and DM Karl (1996a) Nitrite distributions and dynamics at Station ALOHA. Deep Sea  
987 Research Part II: Topical Studies in Oceanography 43, 385-402

988 Dore, JE and DM Karl (1996b) Nitrification in the Euphotic Zone as a Source for Nitrite, Nitrate,  
989 and Nitrous Oxide at Station ALOHA. Limnology and Oceanography 41, 1619-1628

990 Duce et al. (2008) Impacts of Atmospheric Anthropogenic Nitrogen on the Open Ocean. Science  
991 320, 893 – 897.

992 Dugdale, R. C. and J. J. Goering (1967), Uptake of new and regenerated forms of nitrogen in  
993 primary productivity. Limnology and Oceanography 12, 196-206.

994 Dugdale, R. C. and F. P. Wilkerson. (1986), The Use of <sup>15</sup>N to Measure Nitrogen Uptake in  
995 Eutrophic Oceans; Experimental Considerations. Limnology and Oceanography 31, 673-  
996 689.

997 Eppley, RW, J. H. Sharp, E. H. Renger, M. J. Perry and W. G. Harrison (1977), Nitrogen  
998 assimilation by phytoplankton and other microorganisms in the surface waters of the  
999 central north Pacific Ocean. Marine Biology 39, 111-120.

1000 Falkowski, P. G (1997), Evolution of the nitrogen cycle and its influence on the biological  
1001 sequestration of CO<sub>2</sub> in the ocean. Nature 387, 272 – 275.

1002 Fan, C., Glibert, P. M., Alexander, J., and Lomas, M. W. (2003), Characterization of urease  
1003 activity in three marine phytoplankton species, *Aureococcus anophagefferens*,  
1004 *Prorocentrum minimum*, and *Thalassiosira weissflogii*, Marine Biology 142, 949–958.

1005 Foster, R. A., A. Paytan, and J. P. Zehr (2009), Seasonality of N<sub>2</sub> fixation and nifH gene  
1006 diversity in the Gulf of Aqaba (Red Sea). Limnology and Oceanography 54, 219–233.

1007 Francis, C. A., J. M. Beman and M. M. M. Kuypers. (2007), New processes and players in the  
1008 nitrogen cycle: the microbial ecology of anaerobic and archaeal ammonia oxidation. The  
1009 ISME Journal 1, 19-27.

1010 Gilbert, P. M., F. Lipschultz, J. J. McCarthy, and M. A. Altabet (1982), Isotope dilution models  
1011 of uptake and remineralization of ammonium by marine plankton. Limnology and  
1012 Oceanography 27, 639-650.

1013 Granger, J. and D. Sigman. (2009), Removal of nitrite with sulfamic acid for nitrate N and O  
1014 isotope analysis with the denitrifier method. Rapid Communication in Mass Spectrometry  
1015 23, 3753–3762.

1016 Granger, J., D. M. Sigman, J. A. Needoba and P. J. Harrison (2004), Coupled Nitrogen and  
1017 Oxygen Isotope Fractionation of Nitrate during Assimilation by Cultures of Marine  
1018 phytoplankton. Limnology and Oceanography 49, 1763-1773.

1019 Granger, J, D. M. Sigman, M. M. Rohde, et al. (2010), N and O isotope effects during nitrate  
1020 assimilation by unicellular prokaryotic and eukaryotic plankton cultures, *Geochimica et*  
1021 *Cosmochimica Acta*. 74, 1030-1040.

1022 Gruber, N., and J. L. Sarmiento (1997), Global Patterns of Marine Nitrogen Fixation and  
1023 Denitrification, *Global Biogeochem. Cycles* 11, 235–266.

1024 Guerrero, M. A., and R. D. Jones (1996), Photoinhibition of marine nitrifying bacteria. I.  
1025 Wavelength-dependent response. *Marine Ecology Progress Series* 141, 183-192.

1026 Hadas, O. and J. Erez (2004), IET Project No. C Nitrogen Fixation in the Gulf of Eilat In M. J.  
1027 Atkinson, Y. Birk and H. Rosenthal [eds.], *Evaluation of Fish Cages in the Gulf of Eilat,*  
1028 a technical report for the Israeli Ministries of Infrastructure Environment and Agriculture.

1029 Hase, C., M. Al-Qutob, Z. Dubinsky, E. A. Ibrahim, B. Lazar, N. Stambler, M. M. Tilzer (2006),  
1030 A system in balance? Implications of deep vertical mixing for the nitrogen budget in the

1031 northern Red Sea, including the Gulf of Aqaba (Eilat). *Biogeosciences Discussions* 3,  
1032 383-408.

1033 Hollibaugh, J. T., and F. Azam (1983), Microbial degradation of dissolved proteins in seawater.  
1034 *Limnology and Oceanography* 28, 1104–1116.

1035 Jackson, G. A. and P. M. Williams (1985), Importance of dissolved organic nitrogen and  
1036 phosphorus to biological nutrient cycling. *Deep Sea Research* 32, 223-235.

1037 Kamennaya, N. A., M. Chernihovsky, and A. F. Post (2008), The cyanate utilization capacity of  
1038 marine unicellular cyanobacteria. *Limnology and Oceanography* 53, 2485-2494.

1039 Karl, D., R. Letelier, L. Tupas, J. Dore1, J. Christian, and D. Hebel (1997), The role of nitrogen  
1040 fixation in biogeochemical cycling in the subtropical North Pacific Ocean. *Nature* 388,  
1041 533-538.

1042 Klotz, M. G, et al. (2006), Complete Genome Sequence of the Marine, Chemolithoautotrophic,  
1043 Ammonia-Oxidizing Bacterium *Nitrosococcus oceani* ATCC 19707. *Applied and*  
1044 *Environmental Microbiology* 72, 6299-6315.

1045 Knapp, A. N., DiFiore, P. J., Deutsch, C., Sigman, D. M. & Lipschultz, F. (2008) Nitrate isotopic  
1046 composition between Bermuda and Puerto Rico: Implications for N<sub>2</sub> fixation in the  
1047 Atlantic Ocean. *Global Biogeochemical Cycles* 22, GB3014,  
1048 doi:10.1029/2007GB003107

1049 Koper, T., A. F. El-Sheikh, J. M. Norton, and M. G. Klotz (2004), Urease-encoding genes in  
1050 ammonia-oxidizing bacteria. *Applied and Environmental Microbiology*, 70, 2342-2348.

1051 Leichter, J.J., A. Paytan, S. Wankel, K. Hanson, S. Miller and M.A. Altabet (2007), Nitrogen and  
1052 oxygen isotopic signatures of subsurface nitrate: evidence of deep water nutrient sources  
1053 to the Florida Keys reef tract. *Limnology and Oceanography* 52, 1258-1267.

1054 Lindell, D. and A. F. Post (1995), Ultraphytoplankton succession is triggered by deep winter  
1055 mixing in the Gulf of Aqaba (Eilat), Red Sea. *Limnology and Oceanography* 40, 1130-  
1056 1141.

1057 Lindell, D., E. Padan, and A. F. Post (1998), Regulation of ntcA Expression and Nitrite Uptake  
1058 in the Marine *Synechococcus* sp. Strain WH 7803. *Journal of Bacteriology* 180, 1878-  
1059 1886.

1060 Lomas, M. W. and P. M. Gilbert (1999), Temperature regulation of nitrate uptake: A novel  
1061 hypothesis about nitrate uptake and reduction in cool-water diatoms. *Limnology and*  
1062 *Oceanography* 44, 556-572.

1063 Lomas, M. W. and P. M. Gilbert (2000), Comparisons of nitrate uptake, storage and reduction in  
1064 marine diatoms and dinoflagellates. *Journal of Phycology* 36, 903-913.

1065 Lomas, M. W. and F. Lipschultz (2006), Forming the primary nitrite maximum: Nitrifiers or  
1066 phytoplankton? *Limnology and Oceanography* 51, 2453–2467.

1067 MacIsaac, J. J. and R. C. Dugdale (1972), Interactions of light and inorganic nitrogen in  
1068 controlling nitrogen uptake in the sea. *Deep Sea Research* 19, 209-232.

1069 Mackey, K. R. M., R. G. Labiosa, M. Calhoun, J. Street, A. F. Post, A. Paytan (2007),  
1070 Phosphorus availability, phytoplankton community dynamics, and taxon-specific  
1071 phosphorus status in the Gulf of Aqaba, Red Sea. *Limnology and Oceanography* 52, 873–  
1072 885.

1073 Mackey, K. R. M., T. Rivlin, A. Grossman, A. F. Post, and A. Paytan (2009), Picophytoplankton  
1074 responses to changing nutrient and light regimes during a bloom. *Marine Biology* 156,  
1075 1531-1546. DOI 10.1007/s00227-009-1185-2.

1076 McCarthy, J. T. (1972), The Uptake of Urea by Natural Populations of Marine Phytoplankton.  
1077 *Limnology and Oceanography*. 17, 738-748 .

1078 McIlvin, M. R., and M. A. Altabet (2005), Chemical conversion of nitrate and nitrite to nitrous  
1079 oxide for nitrogen and oxygen isotopic analysis in freshwater and seawater. *Analytical*  
1080 *Chemistry* 77, 5589 -5595.

1081 Meeder, E. KRM Mackey, A Paytan, Y Shaked, D Iluz, N Stambler, T Rivlin, AF Post 2, B  
1082 Lazar. Nitrite dynamics in the open sea – A lesson from the northern Red Sea. In press  
1083 *Marine Ecology Progress Series*.

1084 Mingawa, M. and E. Wada. (1986), Nitrogen isotope ratios of red tide organisms in the East  
1085 China Sea: A characterization of biological nitrogen fixation. *Marine Chemistry* 19, 245-  
1086 259.

1087 Montoya, J. P., C. M. Holl, J. P. Zehr, A. Hansen, T. A. Villareal & D. G. Capone (2004), High  
1088 rates of N<sub>2</sub> fixation by unicellular diazotrophs in the oligotrophic Pacific Ocean. *Nature*  
1089 430:1027-1032 doi:10.1038/nature02824.

1090 Moore, L. R., A. F. Post, G. Rocap and S. W. Chisholm. (2002), Utilization of Different  
1091 Nitrogen Sources by the Marine Cyanobacteria *Prochlorococcus* and *Synechococcus*.  
1092 *Limnology and Oceanography*, 47, 989-996.

1093 Needoba, J. A. and P. J. Harrison. (2004), Influence of low light and a light: dark cycle on nitrate  
1094 uptake, intracellular nitrate, and nitrogen isotope fractionation by marine phytoplankton.  
1095 *Journal of Phycology* 40, 505-516.

1096 Olson, R. (1981), Differential photoinhibition of marine nitrifying bacteria: A possible  
1097 mechanism for the formation of the primary nitrite maximum. *Journal of Marine*  
1098 *Research* 39, 227–238.

1099 Opsahl, S. and R. Benner. (1997), Distribution and cycling of terrigenous dissolved organic  
1100 matter in the ocean. *Nature* 386, 480–482.

1101 Palenik, B., and F. M. Morel (1990), Amino acid utilization by marine phytoplankton—a novel  
1102 mechanism. *Limnology and Oceanography* 35, 260-269.

1103 Pantoja, S., D. J. Repeta, J. P. Sachs and D. M. Sigman (2002), Stable isotope constraints on the  
1104 nitrogen cycle of the Mediterranean Sea water column. *Deep-Sea Research I* 49, 1609-  
1105 1621.

1106 Post, A. F., Z. Dedej, R. Gottlieb, H. Li, D. N. Thomas, M. Elabsawi, A. El-Naggar, M. El-  
1107 Gharabawi, and U. Sommer. (2002), Spatial and temporal distribution of *Trichodesmium*  
1108 spp. in the stratified Gulf of Aqaba, Red Sea. *Marine Ecology Progress Series* 239, 241–  
1109 250.

1110 Probyn T. A. and S. J. Painting. (1985), Nitrogen Uptake by Size-Fractionated Phytoplankton  
1111 Populations in Antarctic Surface Waters. *Limnology and Oceanography* 30, 1327-1332.

1112 Robertson, L. A., T. Dalsgaard, N.-P. Revsbeck, and J. G. Kuenen. (1995), Confirmation of  
1113 aerobic denitrification in batch cultures, using gas chromatography and <sup>15</sup>N mass  
1114 spectrometry. *FEMS Microbiology Ecology* 18, 113-120.

1115 Sanudo-Wilhelmy, S. A. et al. (2001), Phosphorus limitation of nitrogen fixation by  
1116 *Trichodesmium* in the central Atlantic Ocean. *Nature* 411, 66–69.

1117 Schreiber, F. B. Loeffler, L. Polerecky, M. M. Kuypers, and D. de Beer  
1118 (2009), <http://www.nature.com/ismej/journal/v3/n11/full/ismej200955a.html> - aff1#aff1  
1119 Mechanisms of transient nitric oxide and nitrous oxide production in a complex biofilm.  
1120 *The ISME Journal* 3, 1301–1313 doi:10.1038/ismej.2009.55.

1121 Sigman, D. M., Altabet, M. A., McCorkle, D. C., Francois, R. & Fischer, G. (2000) The  $\delta^{15}\text{N}$  of  
 1122 nitrate in the Southern Ocean: Nitrogen cycling and circulation in the ocean interior.  
 1123 Journal of Geophysical Research 105 (C8), 19599-19614

1124 Sigman, D. M., J. Granger, P. J. DiFiore, M. M. Lehmann, R. Ho, G. Cane, and A. van Geen  
 1125 (2005), Coupled nitrogen and oxygen isotope measurements of nitrate along the eastern  
 1126 North Pacific margin, Global Biogeochemical Cycles, 19, GB4022,  
 1127 doi:10.1029/2005GB002458.

1128 Smayda, T. J. and B. Mitchell-Innes (1974), Dark survival of autotrophic, planktonic marine  
 1129 diatoms. Marine Biology 25, 195-202.

1130 Solomon, C. M., J. L. Collier, G. M. Berg, P. M. Glibert (2010), Role of urea in microbial  
 1131 metabolism in aquatic systems: a biochemical and molecular review. Aquatic Microbial  
 1132 Ecology. 59, 67–88.

1133 Starkenburg, S. R. (2006). Complete Genome Sequence of *Nitrobacter hamburgensis* X14 and  
 1134 Comparative Genomic Analysis of Species within the Genus *Nitrobacter*. Applied and  
 1135 Environmental Microbiology 74, 2852-2863.

1136 Stepanauskas, R., H. Edling, and L. J. Tranvik (1999), Differential dissolved organic nitrogen  
 1137 availability and bacterial aminopeptidase activity in limnic and marine waters. Microbial  
 1138 Ecology 38, 264–272.

1139 Su, J.-J., B.-Y. Liu, and D.-Y. Liu. (2001), Comparison of aerobic denitrification under high  
 1140 oxygen atmosphere by *Thiosphaera pantotropha* ATCC 35512 and *Pseudomonas stutzeri*  
 1141 SU2 newly isolated from the activated sludge of a piggery wastewater treatment system.  
 1142 Journal of Applied Microbiology 90, 457-462.

1143 Tupas, L. M., I. Koike, D. M. Karl, and O. Holmhansen. (1994), Nitrogen metabolism by  
 1144 heterotrophic bacterial assemblages in Antarctic coastal waters. Polar Biol. 14, 195-204.

1145 Wankel, S. D., Y. Chen, C. Kendall, A. F. Post, A. Paytan. (2009), Sources of aerosol nitrate to  
 1146 the Gulf of Aqaba: Evidence from  $[\delta^{15}\text{N}]$  and  $[\delta^{18}\text{O}]$  of nitrate and trace metal  
 1147 chemistry. Marine Chemistry: 120, 90-99.

1148 Wankel, S. D., C. Kendall, J. T. Pennington, F. P. Chavez, and A. Paytan (2007), Nitrification in  
 1149 the euphotic zone as evidenced by nitrate dual isotopic composition: Observations from  
 1150 Monterey Bay, California, Global Biogeochemical Cycles, 21,  
 1151 GB2009,doi:10.1029/2006GB002723.

1152 Wankel, S. D., C. Kendall, and A. Paytan. (2009), Using nitrate dual isotopic composition ( $\delta^{15}\text{N}$   
 1153 and  $\delta^{18}\text{O}$ ) as a tool for exploring sources and cycling of nitrate in an estuarine system:  
 1154 Elkhorn Slough, California. Journal of Geophysical Research, 114, G01011,  
 1155 doi:10.1029/2008JG000729.

1156 Ward, B. B. (2005), Temporal variability in nitrification rates and related biogeochemical factors  
 1157 in Monterey Bay California, USA, Marine Ecology Progress Series. 292, 97–109.

1158 Ward, B. B. (1985), Light and substrate concentration relationships with marine ammonium  
 1159 assimilation and oxidation rates. Marine Chemistry 16, 301-316.

1160 Ward, B. B., and A. F. Carlucci. (1985) Marine ammonia-oxidizing and nitrite-oxidizing  
 1161 bacteria—serological diversity determined by immunofluorescence in culture and in the  
 1162 environment. Applied Environmental Microbiology 50, 194-201.

1163 Ward, B. B., K. A. Kilpatrick, E. Renger, and R. W. Eppley. (1989), Biological nitrogen cycling  
 1164 in the nitracline. Limnology and Oceanography 34, 493-513.

- 1165 Ward, B. B., R. J. Olson, and M. L. Perry. (1982), Microbial nitrification rates in the primary  
1166 nitrite maximum off southern California. *Deep Sea Research Part A. Oceanographic*  
1167 *Research Papers* 29, 247-255.
- 1168 Wheeler, P. A. and D. L. Kirchman (1986), Utilization of inorganic and organic nitrogen by  
1169 bacteria in marine systems. *Limnology and Oceanography* 31, 998-1009.
- 1170 Wuchter C., B. Abbas, M. J. Coolen, L. Herfort, J. van Bleijswijk, P. Timmers, M. Strous, E.  
1171 Teira, G. J. Herndl, J. J. Middelburg, S. Schouten, and J. S. Sinninghe Damsté (2006),  
1172 Archaeal nitrification in the ocean, *Proceedings of the National Academy of Science*  
1173 *USA* 103, 12317–12322.
- 1174 Zafiriou, O, and M. True (1979), Nitrate photolysis in seawater by sunlight. *Marine Chemistry* 8,  
1175 9–32.
- 1176 Zehr, J. P. and B. B. Ward (2002), Nitrogen Cycling in the Ocean: New Perspectives on  
1177 Processes and Paradigms. *Applied and Environmental Microbiology*, 68, 1015-1024.
- 1178 Zubkov, M. V., B. M. Fuchs, G. A. Tarran, P. H. Burkill, & R. Amann (2003), High Rate of  
1179 uptake of organic nitrogen compounds by *Prochlorococcus* cyanobacteria as a key to their  
1180 dominance in oligotrophic oceanic waters, *Applied and Environmental Microbiology* 69,  
1181 1299–1304 .

1182 **Figure Captions**

1183  
1184 Figure 1: The N cycle under oxic conditions, showing pathways and isotope effects of major N  
1185 transformation processes (Casciotti 2009 and references therein). “ND” indicates that the isotope  
1186 effect has not been determined.

1187  
1188 Figure 2: Depth profiles of  $\text{NO}_3^-$  (shaded area),  $\text{NO}_2^-$  (black line), and chl *a* (green line) for  
1189 January - December in (A) 2008 when the water column mixed down to the seafloor, and (B)  
1190 2003 when the mixing depth was ~400 m. During winter mixing  $\text{NO}_2^-$  accumulates and chl *a* is  
1191 homogenously distributed in the mixed layer, regardless of the mixing depth. During summer  
1192 stratification a PNM forms at or below the DCM. The euphotic depth is ~60 m in winter and  
1193 ~100 m in summer.

1194  
1195 Figure 3: Depth profiles collected at station A before (March 18) and during (March 24 and 25)  
1196 the spring stratification event in 2008 showing (A)  $\text{NO}_3^-$ ,  $\text{NO}_2^-$ ,  $\text{NH}_4^+$ , and chl *a* concentrations.  
1197 The red arrow shows the location of the  $\text{NH}_4^+$  peak that was consumed during nitrification (see  
1198 also Fig. 8D). (B) Cumulative N inventories of particulate N and DIN for depth transects  
1199 collected at station A before (March 18) and during (March 24 and 25) the spring stratification  
1200 event in 2008. (C) Total N inventories for depth transects collected at station A on March 24 and  
1201 25.

1202  
1203 Figure 4: Cell abundances of *Synechococcus*, nanophytoplankton, picoeukaryotes, and non-  
1204 photosynthetic microbes on March 24 (closed circles) and 25 (open circles). Note that different  
1205 scales are used for each group.

1206  
1207 Figure 5: Isotopic composition of N+N and PON on March 18, 24, and 25, showing (A)  $\delta^{15}\text{N}_{\text{N+N}}$ ,  
1208 (B)  $\delta^{18}\text{O}_{\text{N+N}}$ , and (C)  $\delta^{15}\text{N}_{\text{PON}}$ . Measured values for N+N are shown with open circles. Data with  
1209 the correction applied to remove the  $\text{NO}_2^-$  signal as described in the text are shown by the grey  
1210 line for  $\delta^{15}\text{N}_{\text{N+N}}$  and  $\delta^{18}\text{O}_{\text{N+N}}$ .

1211  
1212 Figure 6: Relationships between  $\delta^{18}\text{O}_{\text{N+N}}$  and  $\delta^{15}\text{N}_{\text{N+N}}$  for (A) March 18, (B) March 24, and (C)  
1213 March 25. Data points are color coded as follows: euphotic zone (red), sub-euphotic zone  
1214 (orange), upper PNM (green), and disphotic zone (black). The lines show the 1:1, 3:1 and 5:1  
1215 slopes anchored to  $\delta^{15}\text{N}_{\text{N+N}}$  of 2.03 ‰ and  $\delta^{18}\text{O}_{\text{N+N}}$  of 5.35 ‰ representing deep water in this  
1216 region (600m, March 18<sup>th</sup>). Data with the correction applied to remove the  $\text{NO}_2^-$  signal (as  
1217 described in the text) plot in a similar distribution, but are not shown in the graph for clarity.

1218  
1219 Figure 7: N assimilation into particulate biomass in the  $^{15}\text{N}$  tracer experiment for treatments  
1220 spiked with A)  $\text{NO}_3^-$ , B) urea, C)  $\text{NO}_2^-$ , and D)  $\text{NH}_4$ . Error bars show standard error and are  
1221 smaller than the symbols when not visible.

1222  
1223 Figure 8:  $\text{NO}_3^-$  reduction to  $\text{NO}_2^-$  by phytoplankton is dependent on light and phytoplankton  
1224 abundance (measured as chl *a*). (A) Light attenuation of photosynthetically active radiation  
1225 (PAR) with depth on March 25 showing the depth where irradiance reached 1% surface PAR;  
1226 designated by dotted arrows; (B) correlation of  $\text{NO}_3^-$  reduction rate with irradiance; (C)  
1227 correlation of chl *a* with irradiance; (D) correlation of  $\text{NO}_3^-$  reduction with chl *a* with the effects

1228 of light removed for both parameters (i.e. residuals are plotted). Analysis of residuals revealed  
1229 that nitrification contributed substantially to  $\text{NO}_2^-$  formation at 120 m (open circle), where the  
1230 data deviates from the best fit line (the best fit is based only on the closed circles).

1231

1232 Figure 9: Schematic diagram showing the principal regions of the  $\text{NO}_2^-$  profile as defined in this  
1233 study. NA indicates that a process is not applicable at that depth.



Figure 1

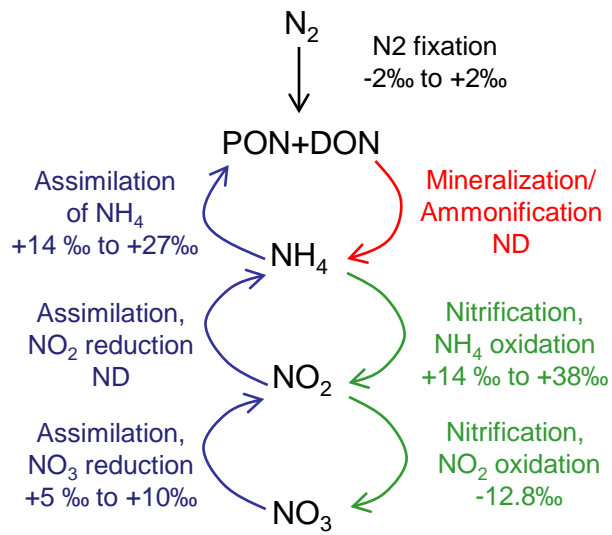


Figure 2

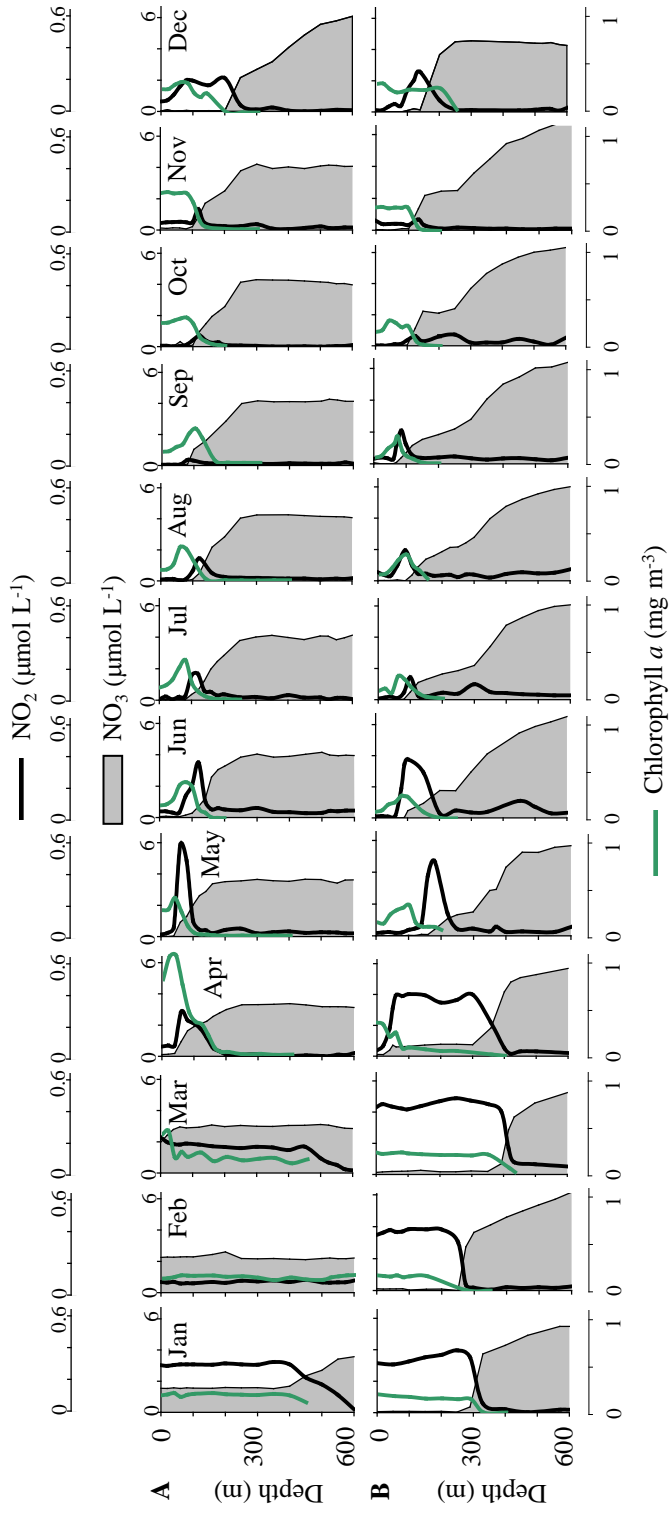


Figure 3

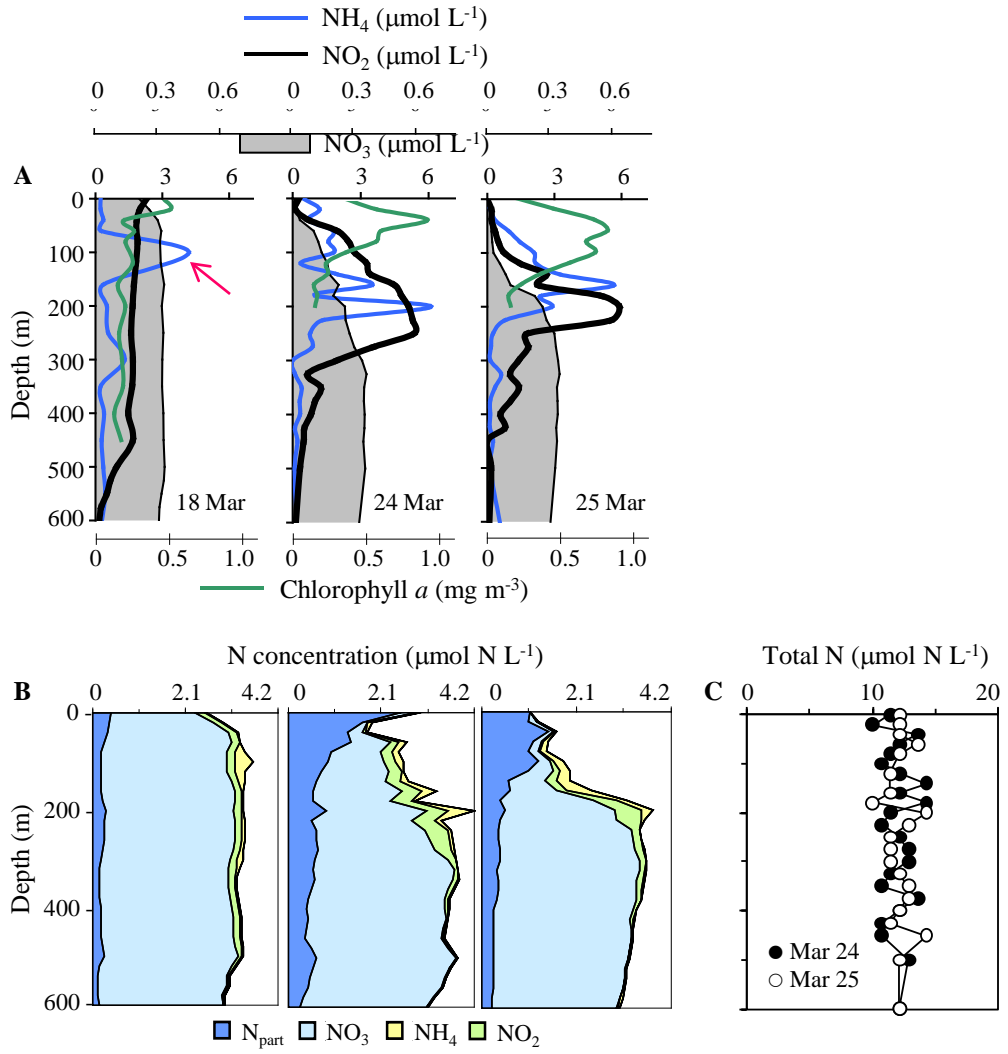


Figure 4

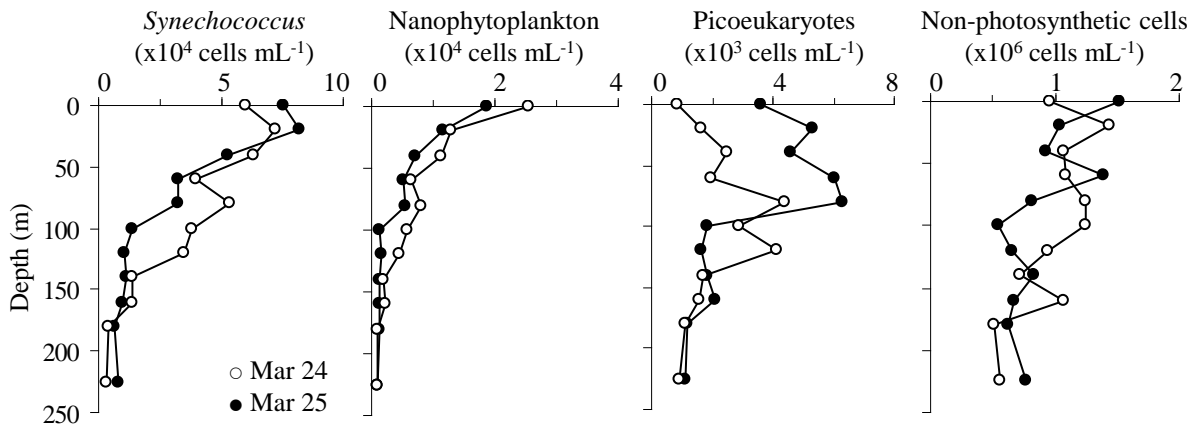


Figure 5

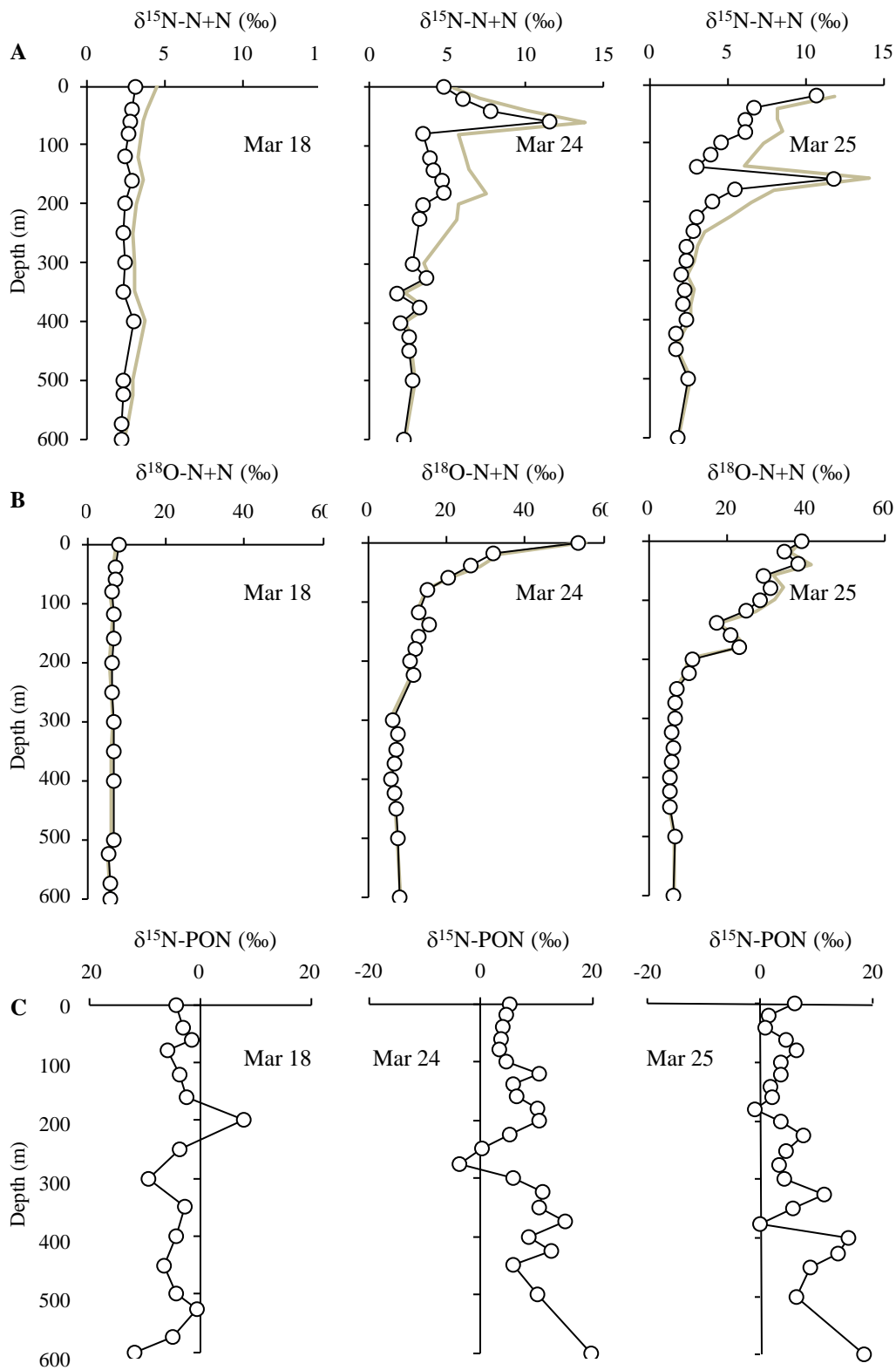


Figure 6

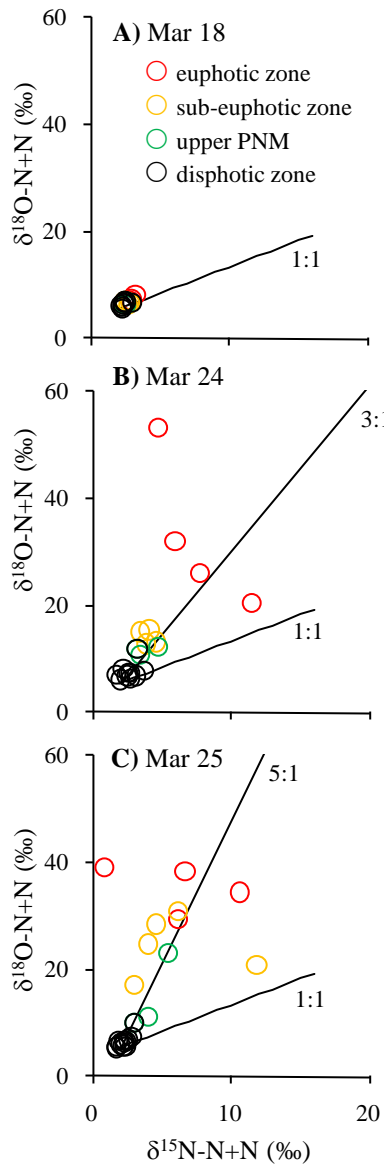


Figure 7

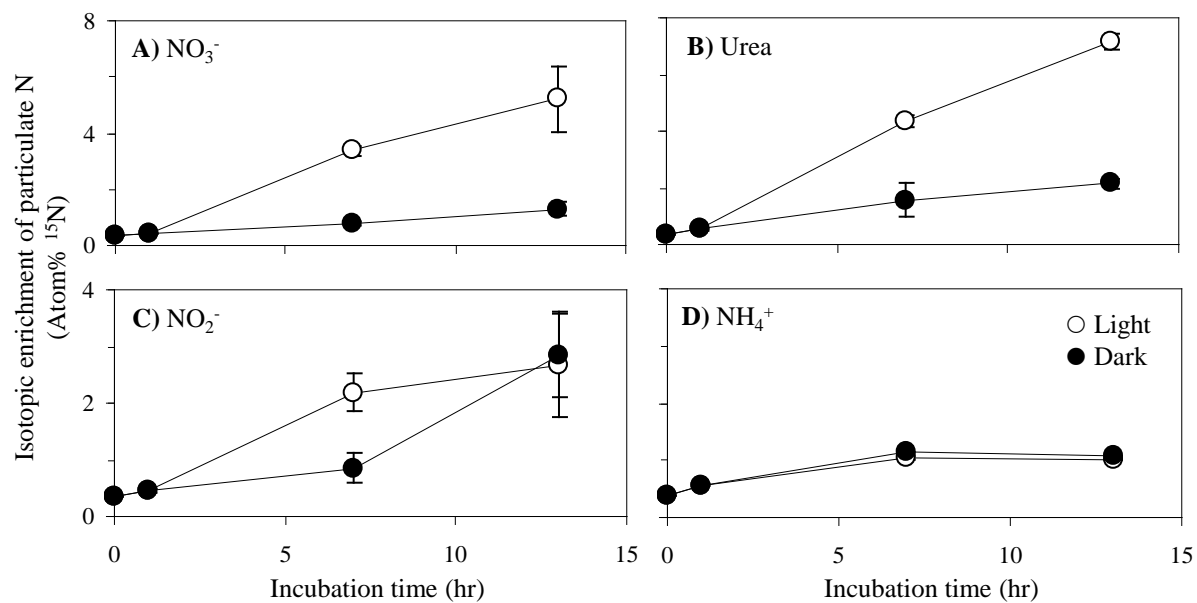


Figure 8

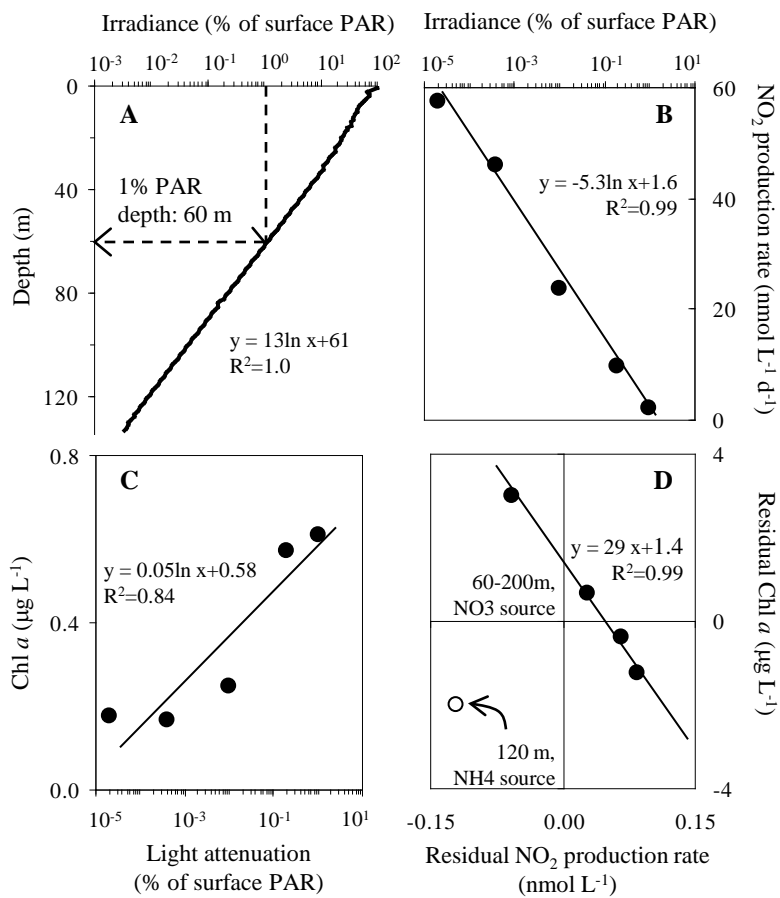




Figure 9

<b>NO<sub>2</sub><sup>-</sup> inventory</b>	<b>Water column region</b>	<b>PAR (%)</b>	<b>Assimilation</b>	<b>NO<sub>3</sub><sup>-</sup> reduction by phytoplankton</b>	<b>Nitrification</b>
	Euphotic zone	>1	maximal	minimal	active; possibly limited to darkness (e.g. at night)
	Sub-euphotic zone	0.001 – 1	minimal	maximal	active; possibly limited to darkness (depth dependent)
	Upper PNM	<0.001	NA	maximal at stratification onset, minimal activity in ongoing stratification	uncoupled; NH <sub>4</sub> <sup>+</sup> oxidation exceeds NO <sub>2</sub> <sup>-</sup> oxidation
	Disphotic zone	<<0.001	NA	NA	coupled; NH <sub>4</sub> <sup>+</sup> oxidation balances NO <sub>2</sub> <sup>-</sup> oxidation